Annu. Rev. Astron. Astrophys. 2001. 39:175–210

THE NEW SOLAR CORONA*

Markus J. Aschwanden[1], Arthur I. Poland[2], and Douglas M. Rabin[2]
[1]Lockheed Martin Advanced Technology Center, Solar and Astrophysics Laboratory, Palo Alto, California 94304, and [2]Laboratory for Astronomy and Solar Physics, NASA Goddard Space Flight Center, Greenbelt, Maryland 20771;
e-mail: aschwanden@lmsal.com, art.poland@gsfc.nasa.gov, douglas.rabin@gsfc.nasa.gov

Key Words magnetic fields, plasma dynamics, coronal heating, solar flares, coronal mass ejections, extreme ultraviolet, soft X rays

■ **Abstract** We focus on new observational capabilities (Yohkoh, SoHO, TRACE), observations, modeling approaches, and insights into physical processes of the solar corona. The most impressive new results and problems discussed in this article can be appreciated from the movies available on the Annual Reviews website and at http://www.lmsal.com/pub/araa/araa.html.

"The Sun is new each day." Heraclites (ca 530–475 BC)
"Everything flows." Heraclites (ca 530–475 BC)

INTRODUCTION

The new solar corona is a restless, intricate, global system. The dynamical richness of the movies from the current generation of solar spacecraft (see Table 1) should be as convincing as any words that follow. These movies illustrate the interaction between spatial scales, from many solar radii to the current limits of angular resolution, and temporal scales, from weeks and perhaps decades to fractions of a second. The dynamics and spatial scales constitute the central challenge of contemporary solar coronal physics. The coronae of other stars seem simpler only through the concealment of distance.

Although the corona's beautiful structure, varying through the solar cycle, has been appreciated since the earliest eclipse observations, physical modeling began with the concept of gravitationally stratified layers (Figure 1, *left*). Within this simple picture it was natural to ask questions. How hot is the corona? What are its radiative, conductive, and advective losses? What heats the gas? How strong is the magnetic field? These questions are still basic, but we can no longer expect

TABLE 1 List of movies[a] available on http://www.lmsal.com/pub/araa/araa.html

Movie 1	Rotating sun in EUV, SoHO/EIT, 195 A, Dec 1996, June 1999
Movie 2	Active region flows, SoHO/CDS, O V 629 A, 27 July 1996, 10 UT
Movie 3	Coronal streamers with comet, SoHO/LASCO, 22 December 1996
Movie 4	Loop oscillations, TRACE, 171 A, 195 A, 14 July 1998, 12:31–12:51 UT
Movie 5	Coronal loops "Fountains of Fire," TRACE, 171 A, 195 A, 6 November 1999, 02:21–04:56 UT
Movie 6	Filament activation, TRACE, 171 A, 29 September 2000, 23:30–00:10 UT
Movie 7	Filament with fan and spine reconnection, TRACE, 171 A, 25 May 1999, 16:48–17:39 UT
Movie 8	Sigmoidal eruptive filament with dimming, TRACE, 171 A, WL, 1600 A, 10 February 2000, 00:11–02:54 UT
Movie 9	2nd Bastille Day flare, TRACE, 171 A, 195 A, 1600 A, 14 July 2000, 10:13–11:09 UT
Movie 10	CME eruption with "particle snow," SoHO/LASCO, 3–6 November 1997
Movie 11	EIT waves after CME (difference movie), SoHO/EIT, 195 A, 12 May 1997, 03:59–07:45 UT
Movie 12	EIT wave after CME (difference movie), SoHO/EIT, 195 A, 7 April 1997, 13:41–17:02 UT

[a]Shows movie event, instrument, wavelengths, and date and time of observations. EUV, extreme ultraviolet; SoHO, Solar and Heliospheric Observatory; EIT, extreme ultraviolet imaging telescope; CDS, coronal diagnostics spectrometer; LASCO, large-angle spectroscopic coronagraph; TRACE, transition region and coronal explorer; CME, coronal mass ejection.

one answer to any of them. The NASA Skylab Mission (1973–1974) revealed a time-variable X-ray corona, including intense bright points, active-region loops, larger scale, apparently diffuse emission, and "coronal holes" (Withbroe & Noyes 1977). Skylab also gave our first clear view of coronal mass ejections (CMEs). The NASA Solar Maximum Mission (1980–1989) added to this picture with observations of spatial structure and flows in the "transition region" (roughly, gas in the temperature range $10^4 < T < 10^6$ K) and with a massive database of coronagraphic observations that emphasized the great importance of CMEs in the dynamic life of the corona and the heliosphere (Strong et al. 1999). Thus, by the 1980s, it was clear that even a first-order understanding of the corona had to take into account large-scale magnetic structure, quasi-stationary flows, and the concentrated nature of magnetic flux in the photosphere (Figure 1, *center*). The 1990s brought three major space observatories (all still operating) that further transformed our view of the corona: Yohkoh, an ISAS/NASA/UK collaboration launched in 1991; the Solar and Heliospheric Observatory (SoHO), an ESA/NASA collaboration launched in 1995; and NASA's Transition Region and Coronal Explorer (TRACE), launched in 1998. These missions, together with other space- and ground-based observations, are developing a picture of the corona that, even at the cartoon level

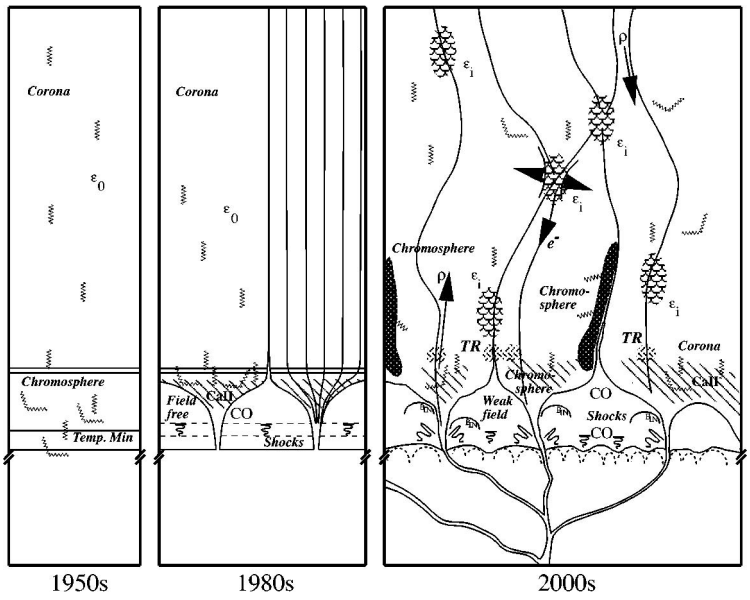

Figure 1 Evolution of the corona cartoon: gravitationally stratified layers in the 1950s (*left*), vertical flux tubes with chromospheric canopies in the 1980s (*middle*), and a fully inhomogeneous mixing of photospheric, chromospheric, transition region (TR), and coronal zones by such dynamic processes as heated upflows, cooling downflows, intermittent heating (ε), nonthermal electron beams (e), field line motions and reconnections, emission from hot plasma, absorption and scattering in cool plasma, acoustic waves, and shocks (*right*). (From Schrijver 2001.)

illustrated in Figure 1 (*right*), is at once intriguing and daunting in its complexity. The traditional terminology of the stratified atmosphere (photosphere, temperature minimum, chromosphere, transition region, corona) has become limiting and confusing. Plotting any physical quantity against height in the atmosphere is an exercise in qualification, except for a specific structure at a particular time. Associating the traditional layers with temperature rather than height is only a little better. The new corona encompasses everything above the photosphere—everything that, in a star peacefully radiating into space, would not be there at all.

This review emphasizes recent observations that have driven us toward a dynamic, multiscale view of the corona. There have also been significant advances in the quantitative measurement of such physical properties as temperature, density, bulk velocity, and chemical composition, together with theoretical advances based on such measurements. Still, some of the "simple" questions about the corona, such as those given above, remain unanswered to a significant extent. This signifies not stagnation in our understanding but a richer, more interesting solar atmosphere: Even simple questions become complex when each is a function of time and place.

THE INHOMOGENEOUS CORONA

The inhomogeneous nature of the solar corona is attributed to its magnetic field. In this section, we discuss the magnetic nature and its impacts on temperature structure.

Magnetic Organization

It is difficult to measure the magnetic field in the corona. Imaging spectroscopy at radio wavelengths is an effective tool immediately above active regions (Bastian et al. 1998a). The Hanle effect can be used to measure the magnetic field in prominences, although both the measurements and their interpretation are delicate (Faurobert-Scholl 1996). Zeeman spectropolarimetry, a highly developed diagnostic of photospheric fields, is handicapped in the corona by lower field strengths and higher temperatures (and thus thermal line widths), although the identification of Zeeman-sensitive lines in the mid-infrared holds promise in conjunction with large-aperture coronagraphs (Kuhn et al. 1999). Despite this, the belief that the magnetic field is the dominant organizing force in the lower corona is well founded. First, the observed distribution of magnetic flux in the photosphere, emerging into a quasi-isothermal (exponential) corona, ensures that magnetic pressure will, on average, exceed static gas pressure up to heights on the order of 100 Mm (Figure 2). Second, although the mathematical problem of inferring the detailed configuration of the coronal magnetic field from well-posed boundary conditions is not completely solved (Amari et al. 1999), a variety of calculational techniques applied to photospheric magnetograms can produce good agreement with observations on scales ranging from active-region loops (Aulanier et al. 2000) to the general configuration of the corona and the speed of the solar wind (Gibson et al. 1999b). The inner corona is undoubtedly a magnetosphere.

Within this framework there remain physical questions of broad astrophysical interest. The distribution of photospheric magnetic flux does not uniquely determine the coronal field, and the corona does not always evolve smoothly in response to changes in photospheric flux. Flares and mass ejections mark impulsive changes in coronal structure. Flares are characterized by a transfer of energy mainly into radiation and fast particles. CMEs reflect the conversion of magnetic into mechanical energy (mass motion and gravitational work) and not necessarily associated with major flaring. So the first questions are why the corona impulsively reorganizes and what determines the manner of reorganization. Another aspect of reorganization is less obvious but equally interesting: What determines the endpoint? Why does the corona often seem to "remember" a previous configuration (for example, by reforming a helmet streamer following a CME)? When the corona reorganizes toward lower magnetic-free energy, it does not ordinarily reach the lowest (potential) configuration.

The decade since Low's (1990) review of coronal magnetic fields has produced considerable insight into these questions while falling short of definitive resolution. From analytic solutions (Low 1992) and numerical models (Antiochos et al. 1994,

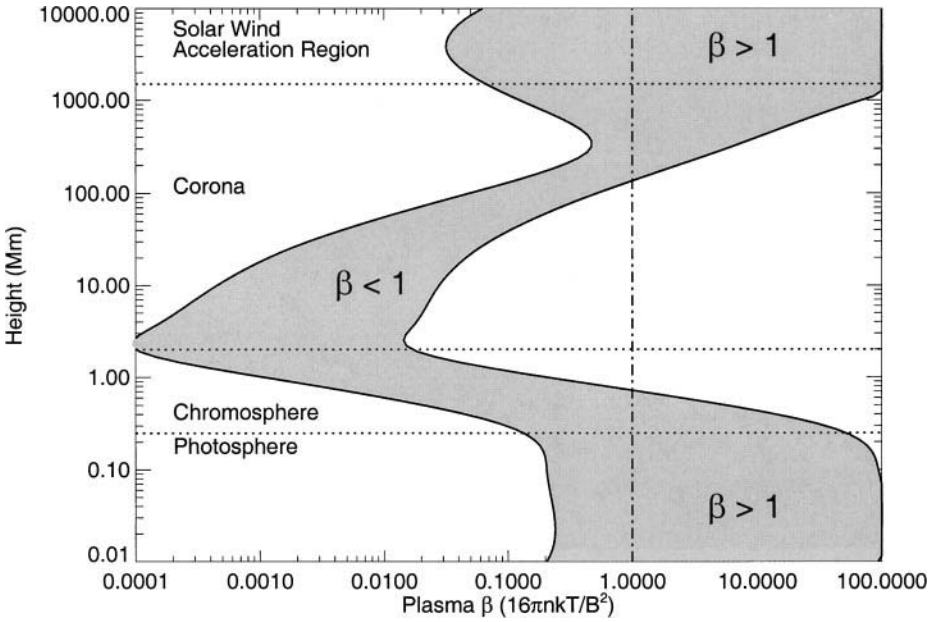

Figure 2 Plasma β in the solar atmosphere for two assumed field strengths, 100 G and 2500 G. In the inner corona ($R \lesssim 0.2 R_\odot$), magnetic pressure generally dominates static gas pressure. As with all plots of physical quantities against height, a broad spatial and temporal average is implied. (Courtesy of G. Allen Gary.)

Démoulin et al. 1996) it has been established that even simple magnetic flux distributions and large-scale motions in the photosphere can produce complex coronal fields with fine-scale structure. The three-dimensional character of these models is essential in producing structure that is not seen in two-dimensional configurations. The actual photospheric magnetic and velocity field is structured and dynamic on all scales from the solar radius to granular convection and subarcsecond flux tubes. Thus, there is no shortage of opportunities for the corona to achieve the kinds of magnetic configurations associated with flares and CMEs. However, the mechanisms responsible for impulsive reorganization are still not established. Parker (1994) has argued extensively that the relative motion of magnetic flux tubes in a highly conductive (frozen-in) plasma leads inevitably to the production of current sheets. It is a separate matter, as yet unresolved, whether the continual dissipation of small-scale current sheets heats closed-field regions of the corona or whether the creation of large-scale sheets destabilizes large-scale magnetic structures.

The concepts of magnetic chirality and helicity have become prominent in the lexicon of solar magnetic fields and may have important consequences for coronal structure and evolution (Rust & Kumar 1996, Canfield et al. 1999). Persistent patterns of twist observed at and above the photosphere may reflect systematic generation of helicity deep in the convection zone. Persistent patterns of chirality

in emerging flux may contribute to the "memory" effect in the corona. Helicity conservation, to the extent that it applies to coronal magnetic fields, may help to explain why impulsive reorganization stops short of the lowest energy state. Also, if CMEs transport helicity away from the Sun, the coronal field may play an essential role in the operation of the solar magnetic dynamo (Low 2000).

On top of this "small-scale" structure, there is a long-term magnetic cycle of approximately 11 years, or a 22-year "Hale cycle," if the alternation of the magnetic polarity is included. During this cycle, the Sun goes from a quiet simple magnetic structure to a very complex multipole and back to a simple almost dipole nature. The Sun is much more dynamic during the more complex period. This can be most easily seen by looking at the movie comparing a month's solar rotation during minimum and near maximum (Movie 1). The movie was made using the extreme ultraviolet imaging telescope (EIT) on SoHO in the coronal line of Fe at 171 Å.

In summary, the coronal magnetic field exhibits a dual nature. Its large-scale structure tends to be persistent and well-predicted by low-order moments of the distribution of magnetic flux at the photosphere. On smaller spatial and temporal scales, the coronal field constantly reorganizes, often violently. Understanding the physical processes involved and unifying this apparent duality is a central goal of coronal physics.

Spatial Complexity

Our observational knowledge of coronal fine structure has increased manyfold in the past decade. The first subarcsecond observations of the corona with the normal incidence X-ray telescope rocket experiment revealed fine strands in loop structures down to the limit of instrumental resolution, $\lesssim 1''$ (Golub et al. 1990). This characteristic has been confirmed by the latest TRACE observations (Schrijver et al. 1999), implying that the transverse spatial scale of elementary heating processes is still unresolved. Fine-scale coronal features resolved with a large optical telescope during a solar eclipse included loop threads down to spatial scales of $0.4''$ (Koutchmy et al. 1994). The fibril or thread-like fine structure complicates physical modeling, requiring unknown filling factors and inhomogeneous models.

A variety of small-scale phenomena have been studied in detail, including transient soft X-ray brightenings (Shimizu et al. 1992), explosive events (Dere et al. 1989, 1991, Chae et al. 1998b,c, 2000a, Winebarger et al. 1999), soft X-ray jets (Shibata et al. 1992, Shimojo et al. 1996, Canfield et al. 1996), extreme ultraviolet (EUV) jets (Wang et al. 1998a, Chae et al. 1999, Brekke 1999, Alexander & Fletcher 1999), bidirectional jets (Innes et al. 1997), blinkers (Harrison et al. 1999), soft X-rays (SXR) network flares and brightenings (Krucker et al. 1997, Falconer et al. 1998), EUV microflares and nanoflares (Berghmans et al. 1998, Krucker & Benz 1999, Parnell & Jupp 2000, Aschwanden et al. 2000c), or the so-called moss structure (DePontieu et al. 1999, Fletcher & De Pontieu 1999, Berger et al. 1999, Martens et al. 2000). These small-scale structures appear to consist of 1–10 Mm bipolar loops (most of the SXR and EUV brightenings, explosive events, microflares, and nanoflares), outflowing plasma collimated along open field lines

(SXR and EUV jets, bidirectional jets), or interfaces of steep temperature gradients between hot coronal loops and the cooler chromosphere (moss), often interleaved with cooler plasma (spicules). The moss structure is localized in a range 2800 $\pm$ 600 km above the photosphere, with a height extension of 1000–3000 km (Fletcher & DePontieu 1999). There is much to be learned from this variety of solar features.

The newly discovered welter of small-scale phenomena in the lower corona shows us that the energization of large-scale coronal structures is often driven by the dynamics of small-scale processes at the base. The opposite, "top-down" scenario, in which large-scale reconfigurations of the magnetic field drive small-scale processes at all levels down to the magnetic foot points, is also at work, as is most evident during flares and CMEs.

Ubiquitous Magnetic Reconnection

"With the observations from Yohkoh, the theoretical concept of magnetic reconnection became a fact." Thus did B. Somov encapsulate the impact of Yohkoh's unblinking observation of the last solar cycle. While the global solar magnetic field, driven by a regenerative dynamo, undergoes a stately oscillation between poloidal and toroidal components, the local magnetic field must constantly adjust to boundary conditions set by subphotospheric flux emergence and connections to interplanetary space. As a consequence of this permanent forcing of the coronal field, the hot plasma seen by Yohkoh traces out an exotic variety of magnetic structures: bipolar loop bundles, helmet-shaped arches (Figure 3*A*), arcades of loops (Figure 3*B*; see also Figure 11), erupting and expanding loops (Figure 3*C*), quadrupolar pairs of loops (Figure 3*D*), cusped loops (Figure 3*E*), fan-like or anemone- type rosettas of loops (e.g., the "bow-tie" in Figure 3*F*), or sinuous chains of helical and S-shaped loops (Figure 3*G*). Other magnetic patterns studied by Yohkoh include transequatorial loops, polar crowns, and shrimp-like loop arcades (Mouradian et al. 1998).

What have we learned from studying this menagerie of magnetic structures? Helmet-streamer and cusp-shaped configurations are considered the most direct evidence of an ongoing reconnection process in a current sheet located between two vertical, antiparallel magnetic field zones (Kopp & Pneuman 1976, Hiei et al. 1993). Reconnection in quadrupolar configurations, where the connectivity between the magnetic poles of opposite signs are exchanged, has been observed in transequatorial loops (Tsuneta 1996) as well as in flares (Hanaoka 1996, Nishio et al. 1997, Aschwanden et al. 1999a). Because two poles of the interacting pair of flare loops could not be resolved observationally, this quadrupolar configuration was initially called a three-legged structure (Hanaoka 1996). Transequatorial loops (Farnik et al. 1999, Delannée & Aulanier 1999, Khan & Hudson 2000), which interconnect foot points from the northern and southern hemispheres, are interesting because they require either a global heating process or transport of heated plasma over huge distances. Because synchronized heating over such large distances is hard to imagine, they probably represent the best separated cases of one-sided (asymmetric) loop-filling and heating.

Sigmoid (S-shaped) magnetic structures have received great attention because of their predictive potential for so-called halo CMEs and subsequent geomagnetic disturbances (Canfield et al. 1999, Rust 1999). The underlying physics of erupting sigmoids may be related to the nonlinear evolution of the kink instability, where reconnection can release more than half of the magnetic free energy stored in the initial equilibrium (Baty 2000a,b).

Recent studies of magnetic reconnection have focused on magnetic separatrices (Démoulin & Priest 1997, Longcope 1998, Longcope & Kankelborg 1999, Brown & Priest 1999, Milano et al. 1999), which are thought to release magnetic energy by current transfer [via magnetic inductance (Melrose 1997)] that can glow in soft X rays. The latest developments focus on such three-dimensional (3D) magnetic reconnection processes as magnetic null points and separatrices in the form of spines and fans (Priest & Forbes 2000, Galsgaard et al. 2000). Filippov (1999) claimed to have observational evidence for a 3D magnetic null point. Aulanier et al. (2000) modeled the magnetic topology of the "Bastille Day" flare (14 July 2000) with the separatrix of a null point. Evidence was inferred (Fletcher et al. 2001) for a 3D nullpoint in a flare trigger site from recent TRACE data. Although many of the cited observations of 3D magnetic structures have been obtained in flare environments, similar processes probably occur undetected in parts of the corona where no hot flare plasma traces out the magnetic structure.

Magnetic modeling of the solar corona has become a minor industry, with no foreseeable bounds in complexity. However, new physical insights typically emerge when new observations uncomfortably restrict the models. The past decade has produced such observations. In the 1980s, mostly photospheric magnetograms alone were used as boundary conditions for extrapolating the coronal magnetic field. We now have high-resolution images from SoHO, Yohkoh, TRACE, and the Very Large Array (VLA), which were used to test the agreement of calculated 3D force-free or magnetohydrodynamic (MHD) field lines with observed field lines as traced by soft X ray or EUV-emitting plasma (e.g., Gary & Alexander 1999, Lee et al. 1999, Aschwanden et al. 1999b). Quite substantial differences were identified that require far more complex magnetic models than potential-field, force-free, or constant-α approximations.

Temperature Inhomogeneities

The EUV and soft X-ray telescopes on SoHO, Yohkoh, and TRACE beautifully elucidate the multitemperature structure of the corona. As Figure 4 illustrates, every wavelength traces out different temperature structures of the solar corona. The coolest temperatures in the corona (except for prominences) are measured in so-called coronal holes, the gateway of open magnetic fields to interplanetary space, where the average electron temperature T_e drops to 0.7–1.3 MK (Habbal et al. 1993, Wilhelm et al. 1998, Chiuderi-Drago et al. 1999, Gibson et al. 1999a). However, a weak high-temperature component has also been detected in coronal holes (Hara et al. 1994, 1996). In the quiet Sun, which is

confined by closed magnetic fields, the temperature averages around 1–2 MK (Alexander 1999, Zhang et al. 1999, Feldman et al. 1999a, Aschwanden & Acton 2001). In active regions, where the average magnetic field and heat input are greater, the average temperature of loops varies between 1 and 8 MK (Kano & Tsuneta 1996, Sterling 1999, Neupert et al. 1998, Lenz et al. 1999), peaking at 10–20 MK during flares. This large observed range of temperature demands that temperature modeling along any given line of sight must take into account the differential emission measure distribution $dEM(T)/dT$ (Landi & Landini 1998). Each instrument, depending on its particular temperature response function, sees only a limited temperature range. Ignoring this instrumental temperature bias in comparing measurements from different instruments (e.g., by using single-temperature models) can lead to temperature discrepancies (e.g., Wolfson et al. 2000).

The brightness temperature of radio observations is generally found to be a factor of two to four lower than the cospatial soft X-ray electron temperature, because of the higher sensitivity of free-free emission at decimetric wavelengths to cooler coronal plasma (Nitta et al. 1991, Schmelz et al. 1992, Brosius et al. 1992, Klimchuk & Gary 1995). Attempts to model the inhomogeneous temperature distribution include two-component models (Zhang et al. 1999), multithread models (Reale & Peres 2000), and gaussian (Aschwanden & Acton 2001) or continuous differential emission measure distributions (Fletcher & DePontieu 1999, Landi & Landini 1998).

A direct consequence of the multitemperature structure of the corona is the multiscale-height effect. Many coronal loops are found to be close to hydrostatic equilibrium (Aschwanden et al. 1999b, Aschwanden & Acton 2001), and gravitational settling is also established for heavier elements (Feldman et al. 1999b). Cooler loops or open field lines with $T_e \approx 1$ MK have a hydrostatic density scale height $\lambda_T = kT/\mu g \lesssim 50$ Mm, whereas hotter loops with $T_e \approx 2$ MK have $\lambda_T \approx 100$ Mm. Given that one is always viewing through multiple loops or structures at various temperatures, determining the average temperature $T(h)$ from density-sensitive filter ratios yields a bias such that the corona appears hotter with increasing altitude, approximately following a temperature average of $T(h) \approx T_0 r/R_\odot$ (Aschwanden & Nitta 2000), even if each loop or field line is isothermal. Instruments with broadband temperature responses (e.g., Yohkoh) are therefore susceptible to this temperature bias, which is negligible for narrowband instruments, such as SoHO/EIT or TRACE. Thus, Yohkoh filter ratios generally show a temperature increase of the corona with altitude (Foley et al. 1996, Sturrock 1996, Sturrock et al. 1996, Wheatland et al. 1997, Acton & Lemen 1998, Fludra et al. 1999). Line-ratio temperatures obtained from different spectral lines [e.g., with the coronal diagnostics spectrometer (CDS)] are susceptible to the same effect and show a temperature increase with height [probably explaining the results of Fludra et al. (1999) and Sterling et al. (1999)].

Other types of temperature measurements confirm the near-isothermality of coronal structures. For example, the method of emission measure loci (Jordan et al. 1987), using Si VII–Si XII spectral lines observed with the instrument for solar

ultraviolet measurement of emitted radiation (SUMER) reveals extremely isothermal structures extending more than a half solar radius in height (Feldman et al. 1999a, Warren 1999). However, temperature determinations from spectral lines of different ions are susceptible to abundance variations (Feldman et al. 1999b) and first-ionization potential effects (Doschek & Laming 2000). Young et al. (1999) report that with CDS they measured no variation of the temperature with height in a plume, whereas a positive temperature gradient was detected in the background, as expected from the hydrostatic weighting bias of a multitemperature background.

In summary, the inhomogeneous solar corona imposes at least two prerequisites for any self-consistent temperature analysis: (*a*) a differential emission measure distribution $dEM(T)/dT$ to account for the multitemperature inhomogeneity, and (*b*) the temperature dependence of density-scale height to account for the height-dependent hydrostatic weighting bias. When flows are included, the complexity increases further.

THE DYNAMIC CORONA

Flows

Quantitative measurements of flow velocities in coronal structures have been mainly obtained by three spectrometers on SoHO (Fleck & Svestka 1997): the CDS instrument, sensing bulk velocities of $\gtrsim$10 km s^{-1}; the SUMER instrument, best suited for detailed line profiles; and the ultraviolet coronagraph spectrometer (UVCS), measuring velocities in the outer corona. The large-angle spectroscopic coronagraph (LASCO), which observes out to 30 $R_\odot$ in visible light, also has made significant contributions to our understanding of flows and the origins of components of the solar wind.

Lower Corona

Recent advances in understanding the lower solar corona are primarily a result of our ability to make simultaneous observations at several temperatures with line profiles and a fairly rapid time cadence. There have been many manifestations of flows in the lower solar corona: upflows of heated plasma, dubbed chromospheric evaporation or ablation (Czaykowska et al. 1999), downflows of cooling plasma and spicular material (Pneuman & Kopp 1978), and unidirectional flows through active-region loops, dubbed siphon flows (McClymont 1989). However, with recent capabilities, we can also observe more dynamical processes, such as downward-propagating compressional waves in the chromosphere (Hansteen 1993), and obtain velocities with more precision over a wider temperature range.

In closed active-region loops, the general picture is that plasma seems to be heated at chromospheric heights, so that coronal upflows (observed as blueshifts) are observed at hotter temperatures ($T_e \gtrsim 0.5$ MK), whereas coronal downflows

(redshifts) are initiated by catastrophic cooling and are thus observed mainly at cooler temperatures ($T_e \lesssim 0.5$ MK). Flows have been measured with velocities $v \approx 50$ km s^{-1}, but they are only present in parts of the loops (Brekke et al. 1997), which may be owing in part to projection and rotation effects. (An example of such flows can be seen in Movie 2, where mass flows and corresponding Doppler shifts in an active-region loop can be seen.) Sheared rotational motion around the loop axes with velocities up to $v \approx 50$ km s^{-1} were clearly measured by Chae et al. (2000b). Although such high velocities are not uncommon (Kjeldseth-Moe & Brekke 1998), they seem to be confined to temperatures $T_e \lesssim 0.5$ MK.

Many TRACE movies show unidirectional flows along active-region loops ($T_e \approx 1$–2 MK), as expected in siphon-flow models with asymmetric heating (e.g., Mariska & Boris 1983, Mariska & Poland 1985), but counterflows are also occasionally observed (Schrijver et al. 1999, Qiu et al. 1999). Typical velocities are in the range $v \approx 30$–100 km s^{-1}, somewhat below the sound speed ($c_s \approx 150$ km s^{-1} at $T_e = 1$ MK).

Some loops show catastrophic cooling, which apparently drops the pressure in the loop top so that the cooled plasma forms clumps (moving at speeds up to 100 km s^{-1}) that fall down to the foot points like coronal rain (accelerated up to one third of surface gravity), emitting in Lyman α and C IV (Schrijver 2001). The flow dynamics at the foot points is not well understood. In downflows at temperatures $T_e \lesssim 0.1$ MK, it was found that the flow-associated enthalpy flux exceeds the thermal conduction heat flow and dominates the overall energy balance in the transition region (Chae et al. 1997). Doppler shift measurements as a function of temperature obtained with SUMER exhibit a peak value of $v = 11$ km s^{-1} at a temperature of $T_e = 0.23$ MK (Chae et al. 1998d, Brekke 1999), which can be modeled by downflows from an upper hot to a lower cool transition region within a converging fluxtube (Rabin 1991).

There are substantial nonthermal velocities present in loops, which can be interpreted in terms of unresolved loop flows, Alfvén waves, or MHD turbulence and thus give scope for testing coronal heating models. Nonthermal line broadening on the order of 5–30 km s^{-1} was measured in SUMER with a maximum around $T_e = 0.3$ MK (Chae et al. 1998a). Dynamic loops (those that exhibit large bulk motions) were found to be distinctly different from stationary loops, in that dynamic loops also exhibit large nonthermal line broadenings (Chae et al. 2000b).

In open-field regions such as coronal holes, mass flows provide the source for the solar wind. SoHO has enabled great progress in measuring outflow velocities in coronal holes. Based on Ne VII velocity maps ($T_e \approx 0.8$ MK, low in the corona), Hassler et al. (1999) found a relationship between outflow velocity and the chromospheric magnetic network structure, which suggests that the solar wind emanates from chromospheric network boundaries and boundary intersections. These Ne VII observations constituted the first two-dimensional images of the velocity structure of coronal holes. The puzzling observation that outflows are only seen at $T_e \approx 0.8$ MK can be modeled with enthalpy-dominated flows in fluxtubes (Poland & Chae 1999).

Outer Corona

When we move significantly off the solar disk, we can determine velocity as a function of height, whereas disk measurements limit us to measuring velocity as a function of temperature. LASCO and UVCS together with Ulysses and SPARTAN-201 have provided unprecedented observations of the flows in the solar corona and in the solar wind. UVCS and SPARTAN-201 have yielded spectral observations out to several solar radii, LASCO has provided white light observations out to 30 $R_{\odot}$, and Ulysses has been able to make in situ measurements in the solar wind out of the ecliptic plane.

The importance of coronal streamers as the source of the solar wind has been a question since the discovery of the solar wind. A major advance in our understanding of this problem has been achieved with observations from UVCS on SoHO. Noci et al. (1997) and Raymond et al. (1997) observed an equatorial coronal streamer in H I Ly α and in O VI. The results are shown in Figure 5. Note the striking difference between the two images of the same streamer. In Ly α, the maximum of intensity is in the core of the streamer and the intensity gradually decreases toward the edges, whereas in the O VI 103.2-nm line, the core is dimmer than the streamer edges. This is likely to be caused by a factor of three depletion of the O VI abundance in the core of the streamer relative to its nearly photospheric abundance along the edges. The deficit seems to be consistent with a gravitational settling of O VI in the closed magnetic field regions in the center of the streamer. An interpretation of this observation is that the central part of the streamer consists of closed loops with low outflow and thus significant settling, whereas the edges of the streamer are open, with an outward flow and, thus, insufficient time for significant settling.

A host of new outflow velocity measurements have been made in coronal holes with UVCS to characterize the fast component of the solar wind (Patsourakos & Vial 2000, Strachan et al. 2000, Giordano et al. 2000). A major result is the observation of large line widths that are the result of anisotropic velocity distributions of H I and O VI. It is seen that above 2 $R_{\odot}$, the O VI transverse speeds and outflow velocities are larger than the corresponding velocities of H I (Kohl et al. 1998, Dobrzycka et al. 1999, Cranmer et al. 1999) (Figure 6). The UVCS intensity measurements over a coronal hole are more consistent with superradial expansion than with radial expansion, as has been noted by other authors. This example of the observed relationship between lighter and heavier elements has significant ramifications for coronal heating and acceleration, as is discussed below.

Using the Ulysses spacecraft, Janardhan et al. (1999) related the electron content in the corona to velocity. When Ulysses was at conjunction in 1991 and 1995, dual-frequency ranging and Doppler observations were conducted through the solar corona. The coronal plasma velocities were determined using a cross-correlation analysis, when tracking data were recorded simultaneously at two well-separated ground stations. It was found that a higher electron density was correlated with a slower outward velocity. In a similar study, using natural radio sources, Kojima et al. (1999) determined that slow solar wind does not arise from closed magnetic

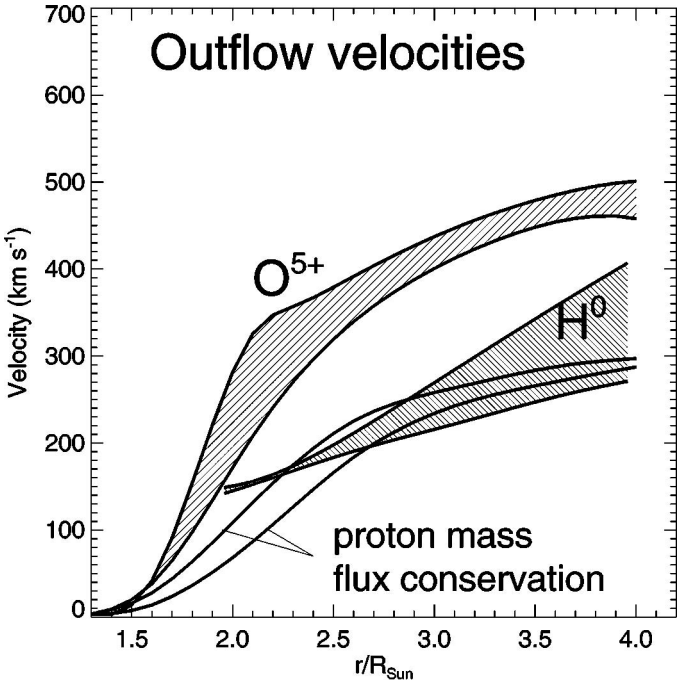

Figure 6 Outflow velocities of neutral hydrogen H^0 (shaded area), ionized oxygen O^{5+} (stippled area), and protons (solid lines), measured with the ultraviolet coronagraph spectrometer over the solar poles in late 1996 and 1997. (From J.L. Kohl.)

loops above an active region, that instead it originates from the vicinity of one polarity side of the active region. This is consistent with the interpretation discussed above.

The coronal observations discussed above are in extremely good agreement with the solar wind in situ measurements, as discussed by Neugebauer (1999), who finds that the speed of the polar solar wind is in the range of 750–800 km s^{-1}, with a slow increase toward the poles. The polar proton flux of approximately 2×10^8 cm^{-2} s^{-1} is only two thirds of the low-latitude flux. The fast, high-latitude wind has less elemental fractionation relative to the solar surface and a lower ionization state than the slow, low-latitude flux. Fine structure in the high-latitude solar wind is currently thought to be the signature of polar plumes seen at the solar surface (Livi et al. 1995).

Direct observation of flows in the low latitude corona have been achieved using the SoHO/LASCO white light coronagraph. This instrument has given us the ability to observe the corona over the range 3–30 $R_\odot$. Sheeley et al. (1997) studied time-lapse sequences to measure the outflow of material in the streamer belt. (Images in the form of a movie showing this effect can be seen in Movie 3.) The authors tracked the outflow of 50–100 inhomogeneities as they traveled from the

Sun. They found the following: (*a*) The inhomogeneities originate 3–4 $R_\odot$ from the solar surface and appear as elongated structures above the cusps of helmet streamers. Their initial sizes are about 1 $R_\odot$ in the radial direction and 0.1 $R_\odot$ in the transverse direction. (*b*) They move radially outward, increasing in length in rough accord with their speeds, which typically doubles from 150 km s^{-1} near 5 $R_\odot$ to 300 km s^{-1} near 25 $R_\odot$. (*c*) Their speed profiles cluster around a nearly parabolic path, yielding an acceleration of about 4 m s^{-2} through most of the 30-$R_\odot$ field of view. This is consistent with an isothermal solar wind expansion at a temperature of approximately 1.1 MK and a sonic point near 5 $R_\odot$. The authors conclude that these features are passively tracing the outflow of the slow solar wind. Further study of these blobs and other features in the corona led Wang et al. (1998b) to deduce that such blobs contribute only a fraction of the slow solar wind and that most originate outside the helmet streamers (i.e., just inside coronal holes). In a further analysis of LASCO data, Tappin et al. (1999) determined that the acceleration to solar wind speeds occurs within the 30-$R_\odot$ LASCO field of view, but with most of the acceleration occurring near the outer part of the field.

These new observations yield a reasonably coherent picture of flows in the corona. At low levels, there are many closed loops with upflows and downflows. Coronal holes provide most of the solar wind and are the source of relatively high speeds. The boundaries of coronal holes, and to a lesser extent streamers, are the source of the slow-speed equatorial wind. The acceleration of the slow-speed wind is accomplished mainly within 30 $R_\odot$ of the solar surface.

Wave Motions

There is growing evidence for the detection of propagating waves in recent high-resolution EUV images of the Sun. The observations in the previous section are believed to indicate mass motion. Here we concentrate on propagating waves, which disturb the local density during the passage of a wave front but do not result in bulk flow. Without spectroscopy, those physically distinct phenomena are hard to separate because they can appear similar in direct images, particularly if the propagating wave is localized (e.g., a shock front or soliton). Recent reviews on this subject can be found from observational (Spadaro 1999) and theoretical (Poedts 1999, Roberts 2000) points of view.

There are essentially three types of propagating waves that have been detected in the solar corona: acoustic waves, MHD (Alvénic, fast, and slow magnetosonic) waves, and shock waves.

The strongest drivers of wave motions are global p-mode oscillations of the solar interior, which can excite upward propagating waves in gravitationally stratified flux tubes passing through the photosphere and chromosphere. Oscillatory signatures of such waves have been detected from power spectra of chromospheric lines with SUMER (Muglach & Fleck 1999, Hansteen et al. 1999, Curdt et al. 1999) and with CDS (Doyle et al. 1997, Brynildsen et al. 1999, 2000), typically with a period within a factor of two of the photospheric 5-min mode. The reality of the upward wave motion was corroborated with blueshift measurements and

phase-shift measurements at different temperatures along the vertical temperature profile. Near sunspots, upward propagating waves are deflected away from the spot, a phenomenon manifested in umbral oscillations and running penumbral waves (for recent work see Alissandrakis et al. 1999, Maltby et al. 1999, BellotRubio et al. 2000, Christopoulou et al. 2000, Tsiropoula et al. 2000, Wikstol et al. 2000).

Do wave motions propagate higher into the corona along closed field lines (loops) or open field lines (plumes)? DeForest & Gurman (1998) report on quasi-periodic wave trains propagating along plumes with outward speeds of 75–150 km s^{-1} and interpret them as compressive (sound or slow-mode MHD) waves (Ofman et al. 1999). Berghmans & Clette (1999) observe similar EUV brightenings propagating with speeds of 75–200 km s^{-1} along active-region loops. After these EIT observations, similar outward propagating disturbances with periods of 3–4 min and speeds of 70–165 km s^{-1} were also observed with TRACE (De Moortel et al. 2000). Although these compressional waves are probably energetically unimportant for the heating of coronal loops [unless they are driven by trapped magnetosonic waves that cause nonlinear steepening (Ofman et al. 1999)], they may provide important diagnostics of dynamic processes at the chromospheric foot points.

In summary, the direct detection of wave motions in coronal structures only became possible with high-cadence EUV observations from EIT and TRACE. The detection of waves opens a new field of coronal seismology, which allows us to probe the coronal magnetic field in situ. Furthermore, the localization of the exciter of coronal waves has the potential to reveal important dynamic processes hidden in the chromosphere.

Loop Oscillations

Magnetic loops are tied firmly only at their two photospheric foot points, while the intervening coronal arch encompasses an elastic plasma torus that is subject to mechanical deformations by external forces. Any disturbance of this elastic plasma torus will be counteracted by a magnetic restoring force, which will result in relaxational oscillations until they are quenched by damping forces. A number of normal-mode (eigen) solutions are known for such harmonic oscillations: (*a*) sausage mode (cross-sectional oscillation), (*b*) kink mode (with transverse amplitudes), (*c*) longitudinal modes; and (*d*) torsional modes (e.g., Roberts et al. 1984, Roberts 2000, and references therein).

Although oscillations have been detected frequently in time profiles of coronal emission, particularly at radio wavelengths after flare episodes, spatially oscillating loops in the corona were not imaged until 2 years ago. The first direct detections of oscillating loops or transverse oscillating magnetic field lines were made by TRACE after flares on 14 July 1998 (Figure 7, see also Movie 4), (Aschwanden et al. 1999c, Nakariakov et al. 1999) and on 4 July 1999 (Schrijver & Brown 2000). Searches for periodic emission from active regions have also been performed in soft X-ray data from Yohkoh (McKenzie & Mullan 1997) and in coronal lines with CDS (O'Shea et al. 1999).

The wave mode of the transverse oscillations detected with TRACE was identified as a fast kink mode (at the fundamental harmonic), which has a period corresponding to the transit time of an Alfvén wave back and forth along the length of the loop, $\tau \approx 2L/v_A$ (Aschwanden et al. 1999c). The oscillation period was found to be close to the helioseismic 5-min period, which suggests a resonant coupling between the photospheric period and the kink mode of the coronal loop. The loop oscillations were triggered by a quasi-radial wavefront that propagated at about 700 km s^{-1} after flare onset. Oscillations were detected in only about six loops out of hundreds in the flaring active region. Obviously, many other loops did not match the kink-mode resonance or were subject to strong damping so that the oscillation did not persist longer than half an oscillation period. For those loops that exhibited transverse oscillations, the oscillating amplitude decayed after two to five periods. This strong damping was interpreted in terms of Alfvénic dissipation by Nakariakov et al. (1999). Assuming viscous damping as the dominant mechanism, they inferred an extremely high Reynolds number that exceeds the predicted classical value by eight to nine orders of magnitude. If this interpretation is correct, coronal heating by viscous dissipation of waves would be much more efficient than previously believed (Nakariakov et al. 1999). However, the mechanism of transverse field line oscillations and their rapid decay could also be reproduced by a rocking of the photospheric foot points, which causes a few loops to oscillate in (anti)phase in the fundamental mode, with a period and decay rate determined by photospheric boundary conditions (Schrijver & Brown 2000) rather than by kink-mode resonance (Aschwanden et al. 1999c). Alternatively, strong damping of standing waves in coronal loops could also be reproduced by foot-point leakage of coronal Alfvén waves due to chromospheric dissipation (B. DePontieu, P.C.H. Martens & H.S. Hudson, submitted) rather than by excessive Reynolds numbers (Nakariakov et al. 1999). Thus, the study of coronal loop oscillations offers not only a diagnostic of the coronal magnetic field, but also upper limits on the coronal viscosity and Reynolds number.

THE CORONAL HEATING PROBLEM

In reviewing recent developments, we follow the approach of Priest (2000) in pursuing the source of coronal heating in two steps: (*a*) localize the heating function and (*b*) identify the heating mechanism that matches this constraint. The latest observations from TRACE provide strong support that the first step is solved now, at least for active-region loops.

Localization of the Coronal Heating Function

When coronal heating mechanisms were reviewed a quarter century ago in this series (Withbroe & Noyes 1977), few observational data were available to constrain the theoretical possibilities.

A pioneering result in terms of a quantitative physical understanding of coronal loops was the Rosner-Tucker-Vaiana (RTV) scaling law (Rosner et al. 1978). They showed that coronal soft X-ray loops observed with Skylab approximately obeyed the relationship $T_{\max} \approx 1400\,(p_0 L)^{1/3}$ (with loop length L, base pressure p_0, and looptop temperature $T_{\max}$) as a consequence of energy balance between heating input, radiative loss, and conductive loss. In its original form, RTV scaling assumed spatially uniform heating along a static loop. Serio et al. (1981) generalized the RTV law to include nonuniform heating functions and gravitation. Recent tests of RTV scaling in statistical samples of soft X-ray loops include Porter & Klimchuk (1995), Kano & Tsuneta (1996), and Kankelborg et al. (1997).

The first attempt to determine the heating function from observations was published by Priest et al. (1998, 2000), using Yohkoh soft X-ray data. Theoretical temperature profiles were calculated from the energy balance between various heating functions and conductive loss and were fitted to the observed filter-ratio temperatures. Because it was observed that the Yohkoh loops show a higher filter-ratio temperature near the loop top than at the foot points, Priest et al. (1998, 2000) concluded that the heating function is concentrated near the loop top, or uniformly distributed, and therefore favored a broadly distributed heating mechanism, such as turbulent reconnection or dissipation of Alfvén waves by turbulent phase mixing. A similar conclusion was reached by Wheatland et al. (1997), who interpreted the temperature increase with height observed by Yohkoh as an indication of downward conduction that implies a heating source high in the corona. However, this interpretation must be viewed cautiously because of the bias present in uncorrected Yohkoh filter ratios that results in an apparent systematic temperature rise with height (Section 2.4) (see also MacKay et al. 2000).

A breakthrough in determining the coronal heating function in loops came with EUV instruments (EIT and TRACE) that have temperature passbands narrow enough to eliminate a significant hydrostatic weighting bias. Neupert et al. (1998) used EIT to measure a nearly isothermal loop and concluded that the data were not consistent with a heating source high in the corona. Similar loop modeling with pseudo-stereoscopic reconstruction (using solar rotation synthesis) applied to EIT data led to the same result: Observed temperature gradients along loops were much shallower than predicted by the RTV model with uniform heating and instead required a nonuniform heating function concentrated toward the loop foot points (Aschwanden et al. 1999b, 2000a). The same deviation of temperature and density profiles from the classical RTV model were confirmed by analyzing loops observed with TRACE (Lenz et al. 1999). Finally, detailed fits of the scaling law of Serio et al. (1981) with nonuniform heating and fits of hydrostatic solutions to 41 TRACE loops favored a heating function confined to the lowest $12{,}000 \pm 5000$ km of the corona, even for loops up to 200,000 km high (Aschwanden et al. 2000b, Schrijver et al. 1999, Aschwanden et al. 2001). This localization of the coronal heating function for loops points toward a mechanism operating at chromospheric and transition region heights.

Many loops in active regions are also found to be far from hydrostatic equilibrium and thus require dynamic models (Figure 8, see also Movie 5). In Figure 8, we show the comparison between observed loops and models of how they would appear if they were in hydrostatic equilibrium. There were efforts to model a TRACE-observed loop with time-dependent hydrodynamic simulations. A qualitative agreement with the observed brightness evolution was found when an initial heating impulse was assumed in an intermediate position between the loop top and one foot point (Reale et al. 2000a,b, Peres 2000). The idea that asymmetric loop heating sets up a dynamic flow is consistent with the modeling of Mariska & Boris (1983) and Mariska & Poland (1985).

In summary, recent observations indicate that heating in coronal loops is often concentrated near their photospheric foot points. However, the localization of heating in open-field regions is equally interesting and still poorly constrained. In both open- and closed-field regions, dynamic models will be increasingly important.

Identification of Coronal Heating Mechanisms

There are a number of new models in which magnetic energization heats plasma to coronal temperatures in the chromosphere or transition region and thus may be responsible for the upflow of coronal material into loops. Flarelike heating of the chromospheric plasma by precipitating nonthermal particles, probably occurring on much lower energy scales than in flares, may also fill coronal loops and open-field lines (Brown et al. 2000). These are manifested as localized transient events, variously termed micro- or nanoflares, according to their size (e.g., Krucker et al. 1997, Benz & Krucker 1998, Berghmans et al. 1998, Parnell & Jupp 2000). On even smaller scales, network-field reconnection events could trigger sudden magnetic relaxations that spring upward quickly and acquire kinetic energy that is dumped into the corona via acoustic waves (Sturrock 1999, Sturrock et al. 1999, Roald et al. 2000). Colliding and reconnecting flux tubes in the photospheric network produce a cascade of shock waves that propagate in different upward directions and can cause explosive instabilities with jets at interaction sites of colliding shock fronts (Ryutova et al. 2001, Tarbell et al. 1999, 2000). This scenario was tested by comparing Doppler shifts measured from SUMER with the predicted shock speeds (Ryutova & Tarbell 2000). The dissipated current of colliding and cancelling magnetic fluxtubes was found to be sufficient to explain the observed intensity of transient soft X-ray brightenings occurring along the intervening magnetic separatrices (Longcope & Kankelborg 1999). Recent numerical MHD simulations also show that the shock waves of colliding chromospheric fluxtubes excite surface and body Alfvén waves suitable for coronal heating (Furusawa & Sakai 2000, Sakai et al. 2000).

As discussed above, loop heating mechanisms that produce a near-uniform heating function or heating concentrated in the upper corona are not consistent with the latest TRACE results. Among proposed coronal heating mechanisms that predict near-uniform or long-range dissipation are (*a*) dissipation of Alfvén waves

(given the low Reynolds number of the corona) and (*b*) most of the DC (electric current) heating mechanisms (by Ohmic dissipation, electric resistivity, viscosity, turbulence). Therefore, these heating mechanisms would be inefficient in the rather homogeneous upper corona. However, density inhomogeneities, mechanical motion, and magnetic braiding and twisting make all these mechanisms more efficient and could make them compatible with the TRACE results, if the driving forces occur in the chromosphere and transition region. Several recent studies point in this direction. Dissipation of Alfvén waves is not found to be an effective heating mechanism for the transition region and corona, but it is probably more efficient in the chromosphere (Campos & Mendes 2000). Whereas the efficiency of resonant absorption heating is low in the homogeneous corona, heating by compression and dissipation of the slow magnetosonic waves and shocks can easily lead to a temperature rise (Bélien et al. 1999). Coronal heating models involving gradual stressing of the magnetic field by foot-point motion are in better agreement with the observed scaling law of the magnetic field than AC wave heating models, such as resonant absorption or current layers (Mandrini et al. 2000).

In summary, progress has been made in solving the first step of the coronal heating problem, i.e., the localization of the coronal heating function, at least for active-region loops. In the second step, however, which heating mechanisms do match this observational constraint and which ones are dominant is still unknown. Some of the mechanisms make specific predictions of the heating efficiency as a function of magnetic geometry, magnetic stressing, helicity, dissipation length, temperature profile, transverse motions, etc. Further quantitative investigations of such quantities, with good spatial and temporal resolution, will be necessary to narrow the range of viable options.

Microflaring and Self-Organized Criticality

Hudson (1991) pointed out that if the frequency distribution of flare energy follows a power law, $N(E) \propto E^{-\alpha}$, and $\alpha < -2$, very small flares (microflares and nanoflares) may provide more heat to the corona than large but infrequent flares. Since then, an enthusiastic search for "microflares" and "nanoflares" has ensued.

The power-law distribution of solar flares has now been measured over eight orders of magnitude, from the largest observed energies of $\lesssim 10^{32}$ ergs down to the detection limit of $\lesssim 10^{24}$ ergs (Figure 9).

Shimizu et al. (1992) and Shimizu & Tsuneta (1997) demonstrated that soft X-ray brightenings detected with Yohkoh represent miniature flares with energies of $\approx 10^{27}-10^{29}$ ergs and have a frequency distribution similar to that of larger flares, with power-law slopes around -1.74. Krucker et al. (1997) analyzed soft X-ray brightenings with even smaller energies ($10^{25}-10^{26}$ ergs) and demonstrated that they have flarelike, nonthermal radio signatures. Krucker & Benz (1998) sampled small EUV brightenings with EIT and derived a frequency distribution with a power-law slope of -2.3 to -2.6, which was the first published value above the critical limit of -2. Parnell & Jupp (2000) confirmed a similar range of

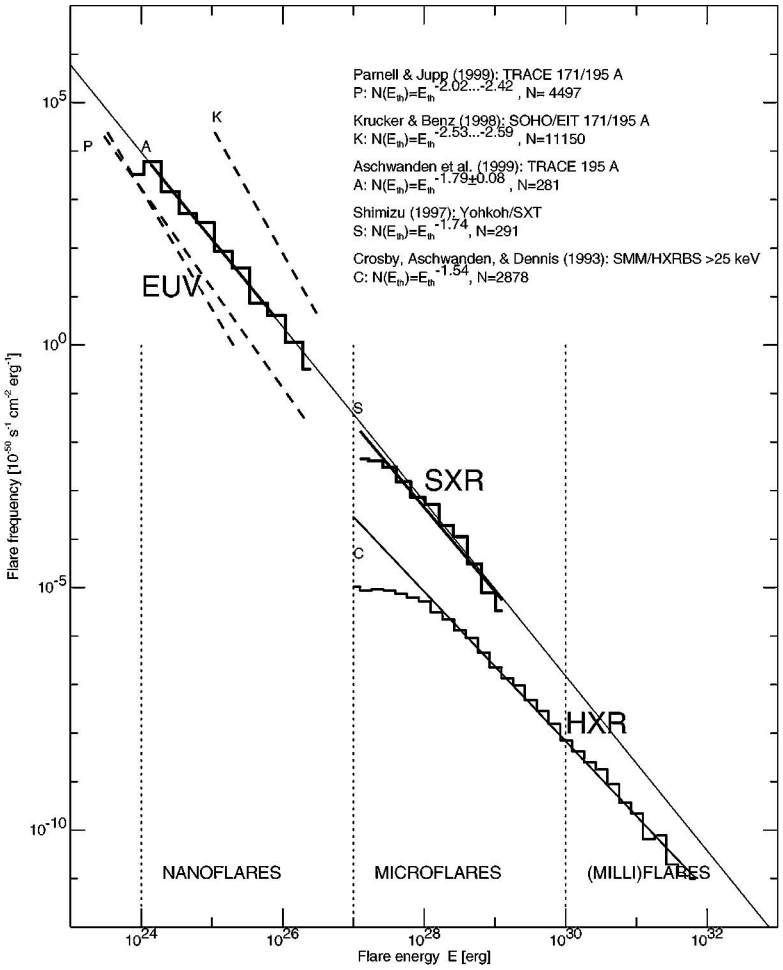

Figure 9 Synthesized frequency distribution of extreme ultraviolet (EUV) nanoflares, soft X-ray microflares, and hard X-ray flares, covering a range of about eight orders of magnitude in energy ($E \approx 10^{24} \ldots 10^{32}$ erg). The combined power-law slope is -1.8, but steeper slopes have been determined for EUV nanoflares in some studies, perhaps indicating a divergence of the energy integral at low energies, which holds the promise that nanoflares could account for a significant fraction of the coronal heating. (Adapted from Aschwanden et al. 2000c.)

power-law slopes, -2.0 to -2.6, by sampling small EUV brightenings recorded with TRACE. However, a more restrictive analysis of EUV brightenings observed with TRACE, discriminating nanoflares from other nonflare brightness changes, revealed a power-law slope around -1.8 (Aschwanden et al. 2000c) (Figure 9). It thus remains controversial whether nanoflares account for enough energy to heat the corona.

Power-law frequency distributions are one of the hallmarks of nonlinear systems with self-organized criticality (Bak et al. 1988). Lu & Hamilton (1991) were the first to apply the concept of self-organized criticality to solar flares and explained their power-law slope of -1.8 with the statistics of small-scale reconnection events that are randomly triggered by nearest-neighbor interactions. A remarkable property of self-organizing systems is that large catastrophes can be triggered by a chain reaction of small random events, regardless of their magnitude. The nonlocal communication of self-organizing models was studied with cellular automata models (MacKinnon et al. 1996, MacKinnon & MacPherson 1997, MacPherson & MacKinnon 1999). Newer work strives for physical models of solar flare avalanches, attempting to tie the dynamics of MHD and/or magnetic reconnection processes to flare energies releases (Vassiliadis et al. 1998, Litvinenko 1998, Isliker et al. 1998, Longcope & Noonan 2000).

Do the largest and smallest flares share the same physical energy release process and exhibit a single power-law slope, or are nanoflares governed by a different process that results in a steeper power-law slope that carries with it the potential for coronal heating (Vlahos 1994, Vlahos et al. 1995)? This issue remains unsettled to date, for several reasons: (*a*) The definition of elementary avalanche events is a subtle and ambiguous data analysis problem, (*b*) the limits of distinct power-law ranges are not known as long as the underlying physical mechanism is not identified, and (*c*) hybrid models of incoherent and coherent random processes can account for almost any combination of exponential and power-law distributions.

The improved resolution and enhanced contrast of EIT and TRACE have shown us really that flarelike processes cover a huge range of eight orders of magnitude in energy. However, whether flarelike processes account also for the coronal heating problem turned out to be delicate statistical problem highly susceptible to methodical uncertainties.

THE ERUPTIVE CORONA

The most dynamic aspects of the corona involve rapid, large-scale magnetic field destabilization. The observational characteristics include CMEs, eruptive filaments, and flares. Arguments about whether flares or eruptive filaments "cause" CMEs are overly narrow in a systems view of the corona. All these observational phenomena are the result of magnetic reorganization; they occur both separately and together, in any combination. They herald the rapid release of large amounts of magnetic energy into thermal energy and radiation, fast particles, and magnetic clouds ejected from the Sun; all of which can directly affect Earth.

Eruptive Filaments

Filaments (referred to as prominences when observed on the solar limb) are clouds of relatively cool material suspended above the solar photosphere (Figure 10). (Movies 6–8 show the dynamics of these features.) They are classified as quiescent prominences when they are not in an active region and are observed to exist at heights in the corona on the order of 50,000 km. Active-region filaments are seen in active regions and are usually low in altitude, only a few thousand kilometers above the surface. Both types are thought to be supported by the magnetic field, which also serves to insulate them from the hot corona. Their characteristic temperature is in the range 5,000–10,000 K.

Filaments are always seen above and along magnetic neutral lines, and there is a strong shear such that the magnetic vector forms an angle of only approximately 20 degrees with the neutral line. One of the concepts describing prominences is well stated in a paper by DeVore & Antiochos (2000): "(1) . . . the sheared core field acquires a dipped geometry that can support cool prominence material against gravity. This confirms previous force-free equilibrium models for forming dipped prominence fields by differential shear and extends them to much larger applied shears and time-dependent dynamics with dissipation. (2) At larger shears, we discover a new mechanism for forming the helical magnetic fields of (quiescent) prominences. It entails a two-step process of magnetic reconnection in the corona. First, flux in the sheared core reconnects with flux in the unsheared, restraining arcade, producing new pairs of interlinked field lines. Second, as these interlinked fields continue to be sheared, they are brought together and reconnect again, producing helical field threading and enveloping the body of the prominence. This mechanism can account for the twist that is often observed in both quiescent and erupting prominences. (3) Even for very large shears, the dipped, helical structure settles into an apparently stable equilibrium, despite the substantial amount of reconnection and twist in the magnetic field. We conclude that neither a kink instability of the helical core field, nor a tether-cutting instability of the restraining arcade, is operating in our low-lying model prominence. This concurs with both observations and a theoretical model for prominence stability." This theoretical model accounts for many (though not all) observed features of filaments.

In a study of the flows in filaments, Zirker et al. (1998) found both streaming and countersteaming along the filament axis (for examples, see Figure 10; see also Movie 6). They observed field-aligned flows with counterstreaming of adjacent flux tubes. We infer from this that the cool material is going up one side of the magnetic tube and down the other, possibly a low, elongated arch-type structure. This does not seem unreasonable for low-lying active-region filaments but is hard to understand for the higher quiescent filaments. Because the scale height of cool material is so small, one would have to push the material up many scale heights in quiescent filaments, requiring large amounts of energy that would not heat. However, Antiochos et al. (1999b) state that their model with dipped magnetic fields can explain the observed motions. We note that none of the observed velocities is consistent with

free fall of cool material at the edges, but following the flow geometry does help significantly with our understanding of the 3D magnetic topology.

Details of quiescent and erupting filaments have been studied in a number of recent observations and models, starting from the subphotospheric origin of filament formation (Jiang & Wang 2000, Rust 2000, Chae et al. 2001b), the photospheric magnetic field structure (VanBallegooijen et al. 1998, 2000, Magara & Kitai 1999, Aulanier et al. 1999), their chirality and helicity (Canfield & Pevtsov 1998, Chae 2000), detailed observations of the chromospheric filament structure with SoHO (Schmieder et al. 1998, 2000, Kucera et al. 1999, Chae et al. 2000c), filament destabilization and eruption (Wang & Sheeley 1999, Su & Su 2000, Wang et al. 2000), their signatures of heated plasma seen in soft X rays (Gopalswamy et al. 1999, Malherbe et al. 1998, Hudson et al. 1999, Singh et al. 1999, Tang et al. 1999, Uchida et al. 1999), and their relationship to interplanetary magnetic clouds (Rust 1999). All in all, the increasing number of filament studies reflects the important role of these structures as tracers of magnetic structure and energy processes in the corona.

The energetics of eruptive prominences has been studied recently by many authors and the results are yielding interesting insights into the instability. Fontenla & Poland (1989) observed that a part of the prominence became mechanically unstable and ejected, while other parts that did not move heated up. Similarly, Kim et al. (2000) observed a filament eruption in conjunction with a flare and magnetic flux changes. Hanaoka & Shinkawa (1999) also observed heating of an eruptive filament associated with a CME. VanBallegooijen & DeLuca (1999) observed a magnetic bubble form as a result of kink instability in the magnetic field that supports the filament. They observed a nearby loop brighten because of particle acceleration and impulsive heating along some of the field lines. Gilbert et al. (2000) reported that the ejected material in eruptive prominences frequently escapes from the bulk of the prominence and returns to the solar surface. They infer that this involves the formation of an X-type neutral line in the region, which allows the disconnection. Plunkett et al. (2000) observed a large polar crown filament that accompanied a well-observed CME. The CME had a clear helical structure identified as a flux rope; the prominence was clearly near the trailing edge of the flux rope. The simulation of a prominence eruption has been achieved in the laboratory by Bellan & Hansen (2000). The direct observation of these processes should lead to significant advancement of our understanding of energy processes occurring on the Sun.

The basic picture we have of a filament is a generally bipolar region that is highly sheared. The effects of shear and helical structure alone do not seem to be sufficient for eruption. The emergence of new flux in the region seems to be important for the formation of an instability. The emergence may yield nothing more than some heating and the "disappearance" of the filament; it may lead to ejection of material from the filament, with no further significant effects; or it may result in heating, ejection, and a complete CME. What is finally observed is as diverse as a summer thunderstorm. Eruptive filaments are a tracer of magnetic instability.

Flares

Solar flares, the most energetic ($10^{29}-10^{32}$ erg) and rapid (variable down to milliseconds) phenomena observed in the solar corona, still challenge our physical understanding of the coronal plasma. How can magnetic energy be dissipated quickly into heating and particle acceleration? How does this unstable chain reaction transform into a wide variety of chromospheric, coronal, interplanetary, and geomagnetic manifestations? The complexity of the problem is reflected in some 2000 observational and theoretical flare studies published over the past 20 years. We refer the reader to recent reviews (Hudson & Ryan 1995, Miller et al. 1995, Sakai & DeJager 1996, Bastian et al. 1998b, Ramaty & Mandzhavidze 1999, Aschwanden 1999, Reames 1999, Priest 2000, Forbes 2000, Parker 2000), proceedings (Bentley & Mariska 1996, Watanabe et al. 1998, Bastian et al. 1999, Ramaty & Mandzhavidze 2000), and textbooks (Strong et al. 1999, Priest & Forbes 2000, Lang 2000). Here we consider only a few recent studies that highlight new aspects.

Although earlier flare models stressed 2D magnetic reconnection processes occurring in current sheets (e.g., Kopp & Pneumann 1976, Hiei et al. 1993), newer models explore 3D magnetic reconnection at null points, spines, fans, and bald patches as possible triggers (Filippov 1999, Priest & Forbes 2000, Aulanier et al. 2000, Fletcher et al. 2001). Sigmoidal coronal structures have also received considerable attention as flare catalysts (Canfield et al. 1999, Aurass et al. 1999).

There is a growing consensus that the dominant particle acceleration mechanism operating in flares involves stochastic acceleration via gyro-resonant wave-particle interaction, a process that can most easily reproduce the observed energies and acceleration times of nonthermal electrons and ions (Miller et al. 1995), whereas shocks associated with CMEs are thought to accelerate interplanetary ions (Reames 1999). The physical understanding of the kinematics and propagation of accelerated electrons has been significantly improved with electron time-of-flight measurements, leading to accurate localizations of particle acceleration sites (Aschwanden 1999).

The traditional chromospheric evaporation model, which predicts upflows on the outer side of the photospheric flare ribbons and downflows on the inner side, has been verified for the first time by blueshift and redshift measurements with CDS and TRACE images (Czaykowska et al. 1999). A follow-up study revealed chromospheric evaporation with a lack of hard X-ray emission in the extended late-flare phase, requiring thermal conduction as a driver rather than precipitating nonthermal particles (Czaykowska et al. 2001). The traditional scenario of two-ribbon flares also predicts the existence of cospatial hard X-ray ribbons, which have now apparently been observed with Yohkoh during the (second) Bastille Day flare [14 July 2000, 10:03 Universal Time (UT)] (Figure 11; see also Movie 9). This finding is comparable to the Yohkoh/HXT discovery of above-the-loop-top hard X-ray sources (Masuda et al. 1994), which represented the first direct localization of particle acceleration sites in flares.

Whereas Yohkoh observations reveal magnetic structures that become filled by heated ($T_e \approx$ 10–20 MK) flare plasma, TRACE observations show the locations of the cooling ($T_e \approx$ 1–2 MK) postflare plasma, often tracing out myriads of fine loops along a two-ribbon arcade (Figure 11). The high resolution of TRACE ($\lesssim 1''$) allows us to study the topology, evolution, and propagation of ongoing magnetic reconnection (Aulanier et al. 2000, Bentley et al. 2000, Fletcher et al. 2001), the fine structure of flare loop arcades (Warren 2000), the energy balance of the heated and cooling flare plasma (Antiochos et al. 2000), the dynamics of oscillating flare loops (Aschwanden et al. 1999c, Nakariakov et al. 1999, Schrijver & Brown 2000), and the electromechanical coupling between the photosphere and transition region (Tarbell et al. 2000, Ryutova & Tarbell 2000).

Simultaneous high-resolution imaging and spectra from HESSI (to be launched in 2001) will considerably enhance the precision of mapping flare-loop foot points from the precipitation sites of energized particles, which, together with the detailed TRACE images of the coronal flare plasma, will ultimately allow us to reconstruct the spatially fragmented energy release region of the unsteady and intermittent magnetic reconnection processes.

Coronal Mass Ejections and Dimming

CMEs were first observed as transient brightenings in the Orbiting Solar Observatory (OSO-7) observations (Tousey 1973) and were photographed with good detail with the Skylab white light coronagraph observations (MacQueen et al. 1974) and later with the Solar Maximum Mission (SMM) coronagraph (Howard et al. 1985, Hundhausen 1988, 1993, 1999, Webb & Howard 1994). The observations from all these spacecraft showed what appeared to be loops accelerating off the solar limb into space. Using data from the P-78 coronagraph (Michels et al. 1980), Sheeley et al. (1997) developed a differencing technique that for the first time showed "halo" CMEs heading toward or away from Earth. This technique has been refined in the SoHO/LASCO data to show great detail in halo CMEs (Figure 12; see also Movie 10). The monograph CMEs gives a broad overview of the solar and interplanetary aspects of CMEs (Crooker et al. 1997).

CMEs are the coronal manifestations of disequilibrium (Section 2.1) or instability (Section 5.2). They can occur together with an eruptive prominence, with a flare, or with no discernable lower-atmospheric manifestation. The magnetic loops and arcades in the solar corona are sometimes highly sheared, indicating significant nonpotential energy in the structure. This energy can be released into mechanical motion or thermal energy. Numerical simulations indicate that magnetic field emerging into the sheared structure can induce an MHD instability that leads to a release of this energy. Using this concept, prominence eruptions and CMEs have been simulated. A potentially startling but controversial discovery in this area is that these eruptions can be global in nature, such that a major fraction of the corona is involved in the instability and eruption (Lyons & Simnett 1999, Howard et al. 1997).

The question of what causes or triggers CMEs has received wide discussion in the literature, but as indicated above, the question itself may be too simple for the coronal system. Certainly the notion that there is a flare behind every CME is not viable (Gosling 1993). However, it can be argued that there is nevertheless a close physical connection between flares and CMEs (Hudson 1999).

One concept for the cause of the eruption is a magnetic reconnection process triggered by the formation of a thin current sheet that develops below the rising filament (e.g., Forbes 2000). The instability of the magnetic field associated with filaments often results in their ejection from the solar surface and yields a CME. The physical process is that magnetic energy stored in the solar corona is rapidly released. This release is often predictable from the evolution of highly nonpotential (sheared) magnetic fields. For example, high-latitude "polar crown" filaments seem to rise slowly over days, then rise rapidly before eruption. The process seems to be nonlinear such that when a critical point is reached, the configuration becomes highly unstable.

Another, but similar, concept to describe the role of eruptive filaments during a CME event has been developed by Antiochos et al. (1999a,b): the "magnetic breakout" model. Initial slow stressing of a magnetic field above a neutral line is thought to occur either through shearing of magnetic foot points or through emergence of new flux. They address a key problem of older models: how to store more energy in the preeruption phase so that sufficient energy is available to open up the closed low-lying field during eruption, to accelerate the mass ejection, and to lift the plasma against gravity. The key feature of the breakout model is a multipolar topology, where magnetic reconnection between a sheared arcade and a neighboring flux system triggers the eruption.

Observational evidence for multipolar topologies comes from large-scale regions (Webb et al. 1997, VanDriel-Gesztelyi et al. 1998), small parasitic polarities (Delannée & Aulanier 1999), and δ-spots (Hu et al. 1996, Innes et al. 1999, Aulanier et al. 2000). Aulanier et al. (2000) used 3D magnetic reconnection and developed a more general version of Antiochos's model: "a magnetic breakout is the opening of initially low-lying sheared fields, triggered by reconnection at a null point that is located high in the corona and that defines a separatrix enclosing the sheared fields." Indirect evidence for this reconnection process comes from the ejection of plasmoids or flux ropes (Shibata et al. 1995, Nitta & Yaji 1997), long-duration soft X-ray events near the onset of CMEs (Sheeley et al. 1983), and restructuring of the corona following a CME release (Hiei et al. 1993).

Combined EIT and LASCO observations have allowed us to trace the evolution of CMEs "from cradle to grave," demonstrating their origin in the lower corona (Dere et al. 1997, Delannée et al. 2000). Such observations also clarify the 3D structure of CMEs, which traditionally were thought to consist of spherical shells or arcades of loops with a shock front surrounding a cavity (e.g., Hundhausen 1999), but now have been partially described as 3D helical structures. Helical magnetic flux ropes (Chen et al. 1997, Wood et al. 1999, Dere et al. 1999) have been related to interplanetary magnetic clouds.

A newly observed phenomenon of CMEs is the dimming of soft X-ray and EUV emission in the neighborhood of the CME origin, which is a direct evidence for the evacuation and upward expansion of coronal mass (Hudson et al. 1996, Sterling & Hudson 1997, Aschwanden et al. 1999c). The first EUV observations of this process in the lower corona were reported by Thompson et al. (1998, 1999, 2000). A wave was observed to propagate through the corona, much as Moreton waves have been observed in the photosphere (Figure 13; see also Movies 11 and 12). Circular or sectoral wave fronts expand quasi-radially with typical velocities of $\approx$250 km s^{-1} over the entire solar disk. The corona exhibits a dimming behind the propagating wavefront, which might be the signature of rarefaction caused by the associated CME. Similar large-scale propagating disturbances have been observed with TRACE in the temperature range of 1.0–1.4 MK but have been interpreted as fast-mode MHD waves (Wills-Davey & Thompson 1999). Similarly, Harrison & Lyons (2000) report the observation of a density decrease in the low corona associated with the activation of an adjacent prominence. From this we conclude that CME material is low coronal material being ejected from the Sun, and there is a global communication in the coronal system evidenced by such waves. The ramifications of this global communication need further study.

In the outer corona, there have been some new discoveries with respect to the acceleration of CMEs. There seem to be two different classes defined by Sheeley et al. (1999): gradual (400–600 km s^{-1}) and impulsive a (500–1000 km s^{-1}). They observed that the faster CMEs decelerate after their initial acceleration, whereas gradual CMEs do not. Lin & Forbes (2000) suggest that the deceleration or lack of deceleration is dependent on the interaction between the rates of current sheet formation and reconnection. The effect may also simply reflect the interaction of the CME with the ambient solar wind. The physics of CME propagation in the outer corona and the solar wind will clearly be an important problem for the future in predicting when a CME will impact Earth.

The interplay between new observations and new theoretical work is illustrated by recent studies on the geometry and dynamics of CMEs in terms of erupting flux rope models (Chen et al. 2000), their helical nature and relation to sigmoidal structures (Amari et al. 2000, Hori 2000, Glover et al. 2000), the MHD dynamics and driving mechanisms (Birn et al. 2000, Cargill et al. 2000, Chen et al. 2000, Krall et al. 2000), the relation of CMEs to radio shock signatures, i.e., type II bursts (Klassen et al. 2000, Magara et al. 2000, Maia et al. 2000), or the acceleration of energetic interplanetary particles by CME shocks (Klein & Trottet 2001, Latinen et al. 2001).

Research on CMEs is a rapidly growing field, fueled by a practical interest in space weather and spawning cross-fertilization between solar, heliospheric, and magnetospheric physics. In the near future (2005), the dual-spacecraft STEREO mission will provide direct 3D information to constrain 3D modeling of CMEs.

OUTLOOK

In one sense, the discovery of this past decade is a rediscovery of what Skylab taught us in 1973: The corona is dynamic. However, the quality of the new observations and the improvement of the theories has been dramatic: "Previously we took pictures of the bird; now we have movies of it flying" (A. Title). We again urge the reader to view the movies linked to this review.

Observationally, many advances have been connected with flows and with the acceleration of CMEs and the solar wind. The velocity and acceleration of the wind is measured to have spatial structure: corona holes, the edges of streamers, and CMEs.

At least in the case of coronal loop systems, the source of coronal heating may finally have been localized, revealing small-scale heating sources located near or in the chromosphere. A key to many of these measurements has been long, uninterrupted periods of observation and good time resolution.

The models have developed from simple 1D to 3D, time-dependent calculations. In many cases, these calculations come tantalizingly close to the observations. However, there is still much to do. Most significantly, we still do not have a reliable diagnostic of physical processes that heat the corona, nor do we know what accelerates the solar wind; and, as indicated in the Introduction, we have fewer reasons than ever to believe that these questions have a single answer.

A fleet of new spacecraft has been developed capable of making significant progress in our physical understanding. The STEREO Mission is designed to make 3D measurements of the solar corona and CMEs. The SOLAR-B spacecraft will observe the Sun with much higher spatial and temporal resolution. It will also make higher-resolution EUV spectra of the corona. The "Living With a Star" program will comprehensively observe the Sun, heliosphere, magnetosphere, and ionosphere to better understand the Sun-Earth system and its impact on society.

ACKNOWLEDGMENTS

We are grateful to B.C. Low for sharing his insights into coronal organization and to O. Engvold and T. Kucera for their comments on prominences.

LITERATURE CITED

Acton LW, Feldman U, Bruner ME, Doschek GA, Hirayama T, et al. 1992. *Science* 258:618–25

Acton LW, Lemen J. 1998. See Watanabe et al. 1998. pp. 15–17

Alexander D. 1999. *J. Geophys. Res.* 104/A5:9701–8

Alexander D, Fletcher L. 1999. *Sol. Phys.* 190:167–84

Alissandrakis CE, Tsiropoula G, Mein P. 1999.

Proc. 9th Eur. Meet. Solar Phys., ed. A Wilson, Noordwijk, Netherlands: Eur. Spa. Agy. 448:217–20
Amari T, Boulmezaoud TZ, Mikic Z. 1999. *Astron. Astrophys.* 350:1051–59
Amari T, Luciani JF, Mikic Z, Linker J. 2000. *Ap. J.* 529:L49–52
Antiochos SK, Dahlburg RB, Klimchuk JA. 1994. *Ap. J.* 420:L41–44
Antiochos SK, DeLuca EE, Golub L, McMullen RA. 2000. *Ap. J.* 542:L151–54
Antiochos SK, DeVore CR, Klimchuk JA. 1999a. *Ap. J.* 510:485–93
Antiochos SK, DeVore CR, Klimchuk JA. 1999b. *Am. Astron. Soc. Meet.* 194:31.02
Aschwanden MJ. 1999. *Proc. 9th Eur. Meet. Solar Phys.*, ed. A Wilson, Noordwijk, Netherlands: Eur. Spa. Agy. 448:1015–24
Aschwanden MJ, Acton LW. 2001. *Ap. J.* 550:475–92
Aschwanden MJ, Alexander D, Hurlburt N, Newmark JS, Neupert WM, et al. 2000a. *Ap. J.* 531:1129–49
Aschwanden MJ, Fletcher L, Schrijver C, Alexander D. 1999c. *Ap. J.* 520:880–94
Aschwanden MJ, Kosugi T, Hanaoka Y, Nishio M, Melrose DB. 1999a. *Ap. J.* 526:1026–45
Aschwanden MJ, Newmark JS, Delaboudiniere JP, Neupert WM, Klimchuk JA, et al. 1999b. *Ap. J.* 515:842–67
Aschwanden MJ, Nightingale RW, Alexander D. 2000b. *Ap. J.* 541:1059–77
Aschwanden MJ, Nitta N. 2000. *Ap. J. Lett.* 535:L59–62
Aschwanden MJ, Schrijver CJ, Alexander D. 2001. *Ap. J.* 550:1036–50
Aschwanden MJ, Tarbell T, Nightingale R, Schrijver CJ, Title A, et al. 2000c. *Ap. J.* 535:1027–46
Aulanier G, DeLuca EE, Antiochos SK, McMullen RA, Golub L. 2000. *Ap. J.* 540:1126–42
Aulanier G, Démoulin P, Mein N, VanDriel-Gesztelyi L, Mein P, Schmieder B. 1999. *Astron. Astrophys.* 342:867–88
Aurass H, Vrsnak B, Hofmann A, Rudzjak V. 1999. *Sol. Phys.* 190:267–93
Bak P, Tang C, Wiesenfeld K. 1988. *Phys. Rev. A* 38(1):364–74
Balasubramaniam KS, Harvey JW, Rabin DM, eds. 1998. *Synoptic Solar Physics*. San Francisco: Astron. Soc. Pac.
Bastian TS, Benz AO, Gary DE. 1998a. *Annu. Rev. Astron. Astrophys.* 36:131–88
Bastian TS, Gary DE, White SM, Hurford GJ. 1998b. See Balasubramaniam et al. 1998. pp. 56–75
Bastian TS, Gopalswamy N, Shibasaki K, eds. 1999. *Proc. Nobeyama Symp.*, Kiyosato, Japan: NRO Rep. 479
Baty H. 2000a. *Astron. Astrophys.* 353:1074–82
Baty H. 2000b. *Astron. Astrophys.* 360:345–50
Bélien AJC, Martens PCH, Keppens R. 1999. *Ap. J.* 526:478–93
Bellan PM, Hansen JF. 2000. *Am. Astron. Soc. SPD Meet.* 32:2.66
BellotRubio LR, Collados M, RuizCobo B, Rodriguez Hidalgo I. 2000. *Ap. J.* 534:989–96
Bentley RD, Klein KL, VanDriel-Gesztelyi L, Démoulin P, Trottet G, et al. 2000. *Sol. Phys.* 193:227–45
Bentley RD, Mariska JT, eds. 1996. *Magnetic Reconnection in the Solar Atmosphere. Astron. Soc. Pac. Conf. Ser. 111*, San Francisco: Astron. Soc. Pac.
Benz AO, Krucker S. 1998. *Sol. Phys.* 182:349–63
Berger TE, DePontieu B, Fletcher L, Schrijver CJ, Tarbell TD, Title AM. 1999. *Sol. Phys.* 190:409–18
Berghmans D, Clette F. 1999. *Sol. Phys.* 186:207–29
Berghmans D, Clette F, Moses D. 1998. *Astron. Astrophys.* 336:1039–55
Birn J, Gosling JT, Hessi M, Forbes TG, Priest ER. 2000. *Ap. J.* 541:1078–95
Brekke P. 1999. *Sol. Phys.* 190:379–408
Brekke P, Kjeldseth-Moe O, Harrison RA. 1997. *Sol. Phys.* 175:511–21
Brosius JW, Willson RF, Holman GD, Schmelz JT. 1992. *Ap. J.* 386:347–58
Brown DS. Priest ER. 1999. *Sol. Phys.* 190:25–33

Brown JC, Krucker S, Guedel M, Benz AO. 2000. *Astron. Astrophys.* 359:1185–94

Brynildsen N, Kjeldseth-Moe O, Maltby P, Wilhelm K. 1999. *Ap. J.* 517:L159–62

Brynildsen N, Maltby P, Leifsen T, Kjeldseth-Moe O, Wilhelm K. 2000. *Sol. Phys.* 191:129–59

Campos LMBC, Mendes PMVM. 2000. *Sol. Phys.* 191:257–80

Canfield RC, Hudson HS, McKenzie DE. 1999. *Geophys. Res. Lett.* 26:627–30

Canfield RC, Pevtsov AA. 1998. See Balasubramaniam. et al. 1998. pp. 131–43

Canfield RC, Reardon KP, Leka KD, Shibata K, Yokoyama T, Shimojo M. 1996. *Ap. J.* 464:1016–29

Cargill PJ, Schmidt J, Spicer DS, Zalesak ST. 2000. *J. Geophys. Res.* 105:7509–20

Chae J. 2000. *Ap. J.* 540:L115–18

Chae J, Denker C, Spirock TJ, Wang H, Goode PR. 2000c. *Sol. Phys.* 195:333–46

Chae J, Martin SF, Yun HS, Kim J, Lee S, et al. 2001b. *Ap. J.* 548:497–507

Chae J, Qiu J, Wang H, Goode PR. 1999. *Ap. J.* 513:L75–78

Chae J, Schühle U, Lemaire P. 1998a. *Ap. J.* 505:957–73

Chae J, Wang H, Goode PR, Fludra A, Schuehle U. 2000a. *Ap. J.* 528:L119–22

Chae J, Wang H, Lee CY, Goode PR, Schühle U. 1998b. *Ap. J.* 497:L109–12

Chae J, Wang H, Lee CY, Goode PR, Schühle U. 1998c. *Ap. J.* 504:L123–26

Chae J, Wang H, Qiu J, Goode PR, Wilhelm K. 2000b. *Ap. J.* 533:535–45

Chae J, Yun HS, Poland AI. 1997. *Ap. J.* 480:817–24

Chae J, Yun HS, Poland AI. 1998d. *Ap. J. Suppl.* 114:151–64

Chen J, Howard RA, Brueckner GE, Santoro R, Krall J, et al. 1997. *Ap. J.* 490:L191–94

Chen J, Santoro RA, Krall J, Howard RA, Duffin R, et al. 2000. *Ap. J.* 533:481–500

Chiuderi-Drago F, Landi E, Fludra A, Kerdraon A. 1999. *Astron. Astrophys.* 348:261–70

Christopoulou EB, Georgakilas AA, Koutchmy S. 2000. *Astron. Astrophys.* 354:305–14

Cranmer SR, Kohl JL, Noci G, Antonucci E, Tondello G, et al. 1999. *Ap. J.* 511:481–501

Crooker N, Josely JA, Feynman J, eds. 1997. *Coronal Mass Ejections*. *AGU Monogr. 99*. Washington, DC: Am. Geophys. Union

Curdt W, Heinzel P, Schmidt W, Tarbell T, von Uexküll M, Wilken V. 1999. *Proc. 9th Eur. Meet. Solar Phys*., ed. A Wilson, Noordwijk, Netherlands: Eur. Spa. Agy. 448:177–82

Czaykowska A, Alexander D, DePontieu B. 2001. *Ap. J.* In press

Czaykowska A, DePontieu B, Alexander D, Rank G. 1999. *Ap. J.* 521:L75–78

DeForest CE, Gurman JB. 1998. *Ap. J.* 501:L217–20

Delannée C, Aulanier G. 1999. *Sol. Phys.* 190:107–29

Delannée C, Delaboudiniere JP, Lamy P. 2000. *Astron. Astrophys.* 355:725–42

DeMoortel I, Ireland J, Walsh RW. 2000. *Astron. Astrophys.* 355:L23–26

Démoulin P, Hénoux JC, Priest ER, Mandrini CH. 1996. *Astron. Astrophys.* 308:643–55

Démoulin P, Priest ER. 1997. *Sol. Phys.* 175:123–55

DePontieu B, Berger TE, Schrijver CJ, Title AM. 1999. *Sol. Phys.* 190:419–35

Dere KP, Brueckner GE, Howard RA, Koomen MJ, Korendyke CM, et al. 1997. *Sol. Phys.* 175:601–12

Dere KP, Bartoe JDF, Brueckner GE. 1989. *Sol. Phys.* 123:41–68

Dere KP, Bartoe JDF, Brueckner GE, Ewing J, Lund P. 1991. *J. Geophys. Res.* 96:9399–407

Dere KP, Brueckner GE, Howard RA, Michels DJ, Delaboudiniere JP. 1999. *Ap. J.* 516:465–74

DeVore CR, Antiochos SK. 2000. *Ap. J.* 539:954–63

Dobrzycka D, Cranmer SR, Panasyuk AV, Strachan L, Kohl JL. 1999. *J. Geophys. Res.* 104(A5):9791–800
Doschek GA, Laming JM. 2000. *Ap. J.* 539:L71–74
Doyle JG, O'Shea E, Erdelyi R, Dere KP, Socker DG, Keenan FP. 1997. *Sol. Phys.* 173:243–58
Falconer DA, Moore RL, Porter JG, Hathaway DM. 1998. *Ap. J.* 501:386–96
Farnik F, Karlicky M, Svestka Z. 1999. *Sol. Phys.* 187:33–44
Faurobert-Scholl M. 1996. *Sol. Phys.* 164:79–90
Feldman U, Doschek GA, Schühle U, Wilhelm K. 1999b. *Ap. J.* 518:500–7
Feldman U, Widing KG, Warren HP. 1999a. *Ap. J.* 522:1133–47
Filippov BP. 1999. *Sol. Phys.* 185:297–309
Fleck B, Svestka Z, eds. 1997. *Sol. Phys.* 170:75–122, 170:143–177, 175:341–570, 175:601–735, Dordrecht: Kluwer Academic
Fletcher L, DePontieu B. 1999. *Ap. J.* 520:L135–38
Fletcher L, Metcalf TR, Alexander D, Ryder LA, Brown DS. 2001. *Ap. J.* In press
Fludra A, DelZanna G, Alexander D, Bromage BJI. 1999. *J. Geophys. Res.* 104(A5):9709–20
Foley CA, Acton LW, Culhane JL, Lemen JR. 1996. *IAU Coll.* 153:419
Fontenla JM, Poland AI. 1989. *Sol. Phys.* 123:143–60
Forbes TG. 2000. *Philos. Trans. R. Acad. Sci. Ser. A* 358:711–27
Furusawa K, Sakai JI. 2000. *Ap. J.* 540:1156–71
Galsgaard K, Priest ER, Nordlund A. 2000. *Sol. Phys.* 193:1–16
Gary A, Alexander D. 1999. *Sol. Phys.* 186:123–39
Gibson SE, Biesecker D, Guhathakurta M, Hoeksema JT, Lazarus AJ, et al. 1999b. *Ap. J.* 520:871–79
Gibson SE, Fludra A, Bagenal F, Biesecker D, DelZanna G, Bromage B. 1999a. *J. Geophys. Res.* 104(A5):9691–700
Gilbert HR, Holzer TE, Burkepile JT, Hundhausen AJ. 2000. *Ap. J.* 537:503–15
Giordano S, Antonucci E, Noci G, Romoli M, Kohl JL. 2000. *Ap. J.* 531:L79–82
Glover A, Ranns NDR, Harra LK, Culhane JL. 2000. *GRL* 27:2161
Golub L, Herant M, Kalata K, Lovas I, Nystrom G, et al. 1990. *Nature* 344:842–44
Gopalswamy N, Nitta N, Manoharan PK, Raoult A, Pick A. 1999. *Astron. Astrophys.* 347:684–95
Gosling JT. 1993. *J. Geophys. Res.* 98:18937–50
Habbal SR, Esser R, Arndt MB. 1993. *Ap. J.* 413:435–44
Hanaoka Y. 1996. *Sol. Phys.* 165:275–301
Hanaoka Y, Shinkawa T. 1999. *Ap. J.* 510:466–73
Hansteen VH. 1993. *Ap. J.* 402:741–55
Hansteen VH, Wikstøl Ø, Carlsson M, Judge P. 1999. *Proc. 8th SoHo Workshop, ESA*, Noordwijk, The Netherlands: Eur. Spa. Agy. 446:351–56
Hara H, Tsuneta S, Acton LW, Bruner ME, Lemen JR, Ogawara Y. 1994. *PASJ* 46:493–502
Hara H, Tsuneta S, Acton LW, Bruner ME, Lemen JR, Ogawara Y. 1996. *Adv. Space Res.* 17(4/5):231–34
Harrison RA, Lang J, Brooks DH, Innes DE. 1999. *Astron. Astrophys.* 351:1115–32
Harrison RA, Lyons M. 2000. *Astron. Astrophys.* 358:1097–108
Hassler DM, Dammasch IE, Brekke P, Curdt W, Mason HE, et al. 1999. *Science* 283: 810
Hiei E, Hundhausen AJ, Sime DG. 1993. *Geophys. Res. Lett.* 20(24):2785–88
Hori K. 2000. *Ap. J.* 543:1011–15
Howard R, Sheeley NR, Koomen MJ, Michels DJ. 1985. *J. Geophys. Res.* 90:8173–91
Howard RA, Brueckner GE, St. Cyr OC, Biesecker DA, Dere KP, et al. 1997. See Crooker et al. 1997, pp. 17–26
Hu FM, Song MT, Liu QZ, Ji MS. 1996. *Sol. Phys.* 165:395–97

Hudson HS. 1991. *Sol. Phys.* 133:357–69
Hudson HS. 1999. *Sol. Phys.* 190:91–106
Hudson HS, Acton LW, Harvey KL, McKenzie DE. 1999. *Ap. J.* 513:L83–86
Hudson HS, Lemen JR, Webb DF. 1996. *Proc. Yohkoh Conf. Observations of Magnetic Reconnection in the Solar Atmosphere. Astron. Soc. Pac. Conf. Ser.*, ed. R Bentley, J Mariska, San Francisco: Astron. Soc. Pac. 111:379–82.
Hudson HS, Ryan J. 1995. *Annu. Rev. Astron. Astrophys.* 33:239–82
Hundhausen AJ. 1988. *Proc. 6th Int. Sol. Wind Conf.* 306:181–214
Hundhausen AJ. 1993. *J. Geophys. Res.* 98:13177–200
Hundhausen AJ. 1999. See Strong et al. 1999. pp. 143–200
Innes DE, Inhester B, Axford WI, Wilhelm K. 1997. *Nature* 386:811–13
Innes DE, Inhester B, Srivastava N, Brekke P, Harrison, et al. 1999. *Sol. Phys.* 186:337–61
Isliker H, Anastasiadis A, Vassiliadis D, Vlahos L. 1998. *Astron. Astrophys.* 335:1085–92
Janardhan P, Bird MK, Edenhofen P, Wohlmuth R, Plettemeier D, et al. 1999. *Sol. Phys.* 184:157–72
Jiang Y, Wang J. 2000. *Astron. Astrophys.* 356:1055–66
Jordan C, Ayres TR, Brown A, Linsky JL, Simon T. 1987. *MNRAS* 225:903–37
Kankelborg CC, Walker ABC, Hoover RB. 1997. *Ap. J.* 491:952–66
Kano R, Tsuneta S. 1996. *Publ. Astron. Soc. Jpn.* 48:535–43
Khan JI, Hudson HS. 2000. *Geophys. Res. Lett.* 27(8):1083
Kim JH, Yun HS, Lee SW, Chae J, Goode PR. 2000. *Am. Astron. Soc. SPD Meet.* 32: 02.67
Kjeldseth-Moe O, Brekke P. 1998. *Sol. Phys.* 182:73–95
Klassen A, Aurass H, Mann G, Thompson BJ. 2000. *Astron. Astrophys. Suppl. Ser.* 141:357–69
Klein KL, Trottet G. 2001. *Space Sci. Rev.* 95: 215–25
Klimchuk JA, Gary DE. 1995. *Ap. J.* 448:925–37
Kohl JL, Noci G, Antonucci E, Toudello G, Huber MCE, et al. 1998. *Ap. J.* 501:L127–30
Kojima M, Fujiki K, Ohmi T, Tokumaru M, Yokobe A, Hakamada K. 1999. *Geophys. Res. Lett.* 104(A8):16993–7004
Kopp RA, Pneuman GW. 1976. *Sol. Phys.* 50:85–98
Koutchmy S, Belmahdi M, Coulter RL, Demoulin P, Gaizauskas V, et al. 1994. *Astron. Astrophys.* 284:249–57
Krall J, Chen J, Santoro R. 2000. *Ap. J.* 539: 964–82
Krucker S, Benz AO. 1998. *Ap. J.* 501:L213–16
Krucker S, Benz AO. 1999. *Sol. Phys.* 191:341–58
Krucker S, Benz AO, Bastian TS, Acton LW. 1997. *Ap. J.* 488:499–505
Kucera TA, Aulanier G, Schmieder B, Mein N, Vial JC. 1999. *Sol. Phys.* 186:259–80
Kuhn JR, MacQueen RM, Streete J, Tansey G, Mann I, et al. 1999. *Ap. J.* 521:478–82
Landi E, Landini M. 1998. *Astron. Astrophys.* 340:265–76
Lang KR. 2000. *The Sun from Space*. Berlin: Springer
Latinen T, Klein KL, Kocharov L, Torsti J, Trottet G, et al. 2001. *Astron. Astrophys.* In press
Lee JW, White SM, Kundu MR, Mikic Z, McClymont AN. 1999. *Ap. J.* 510:413–21
Lenz DD, DeLuca EE, Golub L, Rosner R, Bookbinder JA. 1999. *Ap. J.* 517:L155–58
Lin J, Forbes TG. 2000a. *J. Geophys. Res.* 105:2375–92
Litvinenko YE. 1998. *Astron. Astrophys.* 339:L57–60
Livi S, Parenti S, Poletto G. 1995. In *Int. Sol. Wind Eight Conf.*, p. 93, Lindau, Germany: Max-Planck-Inst.
Longcope DW. 1998. *Ap. J.* 507:433–42
Longcope DW, Kankelborg CC. 1999. *Ap. J.* 524:483–95

Longcope DW, Noonan EJ. 2000. *Ap. J.* 542: 1088–99
Low BC. 1990. *Annu. Rev. Astron. Astrophys.* 28:491–524
Low BC. 1992. *Ap. J.* 399:300–12
Low BC. 2000. *J. Geophys. Res.* In press
Lu ET, Hamilton RJ. 1991. *Ap. J.* 380:L89–92
Lyons MA, Simnett GM. 1999. *Sol. Phys.* 186:363–79
MacKay DH, Galsgaard K, Priest ER, Foley CR. 2000. *Sol. Phys.* 193:93–116
MacKinnon AL, MacPherson KP. 1997. *Astron. Astrophys.* 326:1228–34
MacKinnon AL, MacPherson KP, Vlahos L. 1996. *Astron. Astrophys.* 310:L9–12
MacPherson KP, MacKinnon AL. 1999. *Astron. Astrophys.* 350:1040–50
MacQueen RM, Eddy JA, Gosling JT, Hildner E, Munro RH, et al. 1974. *Ap. J.* 187:L85–88
Magara T, Chen P, Shibata K, Yokoyama T. 2000. *Ap. J.* 538:L175–78
Magara T, Kitai R. 1999. *Ap. J.* 524:469–82
Maia D, Pick M, Vourlidas A, Howard R. 2000. *Ap. J.* 528:L49–51
Malherbe JM, Schmieder B, Mein P, Mein N, VanDriel-Gesztelyi L, VonUexkuell M. 1998. *Sol. Phys.* 180:265–84
Maltby P, Brynildsen N, Fredvik T, Kjeldseth-Moe O, Wilhelm K. 1999. *Sol. Phys.* 190:437–58
Mandrini CH, Démoulin P, Klimchuk JA. 2000. *Ap. J.* 530:999–1015
Mariska JT, Boris JP. 1983. *Ap. J.* 267:409–20
Mariska JT, Poland AI. 1985. *Sol. Phys.* 96: 317–30
Martens PCH, Kankelborg CC, Berger TE. 2000. *Ap. J.* 537:471–80
Masuda S, Kosugi T, Hara H, Tsuneta S, Ogawara Y. 1994. *Nature* 371:495–97
McClymont AN. 1989. *Ap. J.* 347:L47–50
McKenzie DE, Mullan DJ. 1997. *Sol. Phys.* 176:127–45
Melrose DB. 1997. *Ap. J.* 486:521–33
Michels DJ, Howard RA, Koomen MJ, Sheeley NR Jr. 1980. In *Radio Physics of the Sun*, ed. MR Kundu, T Gergely, pp. 439–42. Dordrecht: Reidel
Milano LJ, Dmitruk P, Mandrini CH, Gomez DO, Démoulin P. 1999. *Ap. J.* 521:889–97
Miller JA, Cargill PJ, Emslie AG, Holman GD, Dennis BR, et al. 1995. *J. Geophys. Res.* 102(A7):14631–59
Mouradian Z, Soru-Escaut I, Hiei E, McAllister AH, Shibasaki K, et al. 1998. *Sol. Phys.* 180:313–29
Muglach K, Fleck B. 1999. *Proc. 8th SoHo Workshop*, eds. J-C Vial, B Kaldeich-Schürmann, Noordwijk, The Netherlands: Eur. Spa. Agy. 446:479–502
Nakariakov VM, Ofman L, DeLuca EE, Davila JM. 1999. *Science* 285:862–64
Neugebauer G. 1999. *Rev. Geophys.* 92(37): 107–26
Neupert WM, Newmark J, Delaboudiuère JP, Thompson BJ, Catura RC, et al. 1998. *Sol. Phys.* 183:305–21
Nishio M, Yaji K, Kosugi T, Nakajima H, Sakurai T. 1997. *Ap. J.* 489:976–91
Nitta N, White SM, Kundu MR, Gopalswamy N, Holman GD, et al. 1991. *Ap. J.* 374:374–85
Nitta N, Yaji K. 1997. *Ap. J.* 484:927–36
Noci G, Kohl JL, Antonucci E, Tondello G, Huber MCE, et al. 1997. *Adv. Space Res.* 20:2219
Ofman L, Nakariakov VM, DeForest CE. 1999. *Ap. J.* 514:441
O'Shea EO, Banerjee D, Doyle JG. 1999. *Proc. 9th Eur. Meet. Sol. Phys.*, ed. A Wilson, Noordwijk, The Netherlands: Eur. Spa. Agy. 448:191–96
Parker EN. 1994. *Spontaneous Current Sheets in Magnetic Fields*. Oxford, UK: Oxford Univ. Press. 420 pp.
Parker EN. 2000. *IAU Symp.* 195:455–59
Parnell CE, Jupp PE. 2000. *Ap. J.* 529:554–69
Patsourakos S, Vial JC. 2000. *Astron. Astrophys.* 359:L1–4
Peres G. 2000. *Sol. Phys.* 193:33–52

Plunkett SP, Vourlidas A, Simberova S, Karlicky M, Kotrc P, et al. 2000. *Sol. Phys.* 194:371–91

Pneuman GW, Kopp RA. 1978. *Sol. Phys.* 57: 49–64

Poedts S. 1999. *Proc. 9th Eur. Meet. Sol. Phys.*, ed. A Wilson, Noordwijk, The Netherlands: Eur. Spa. Agy. 448:167–76

Poland AI, Chae J. 1999. *Bull. Am. Astron. Soc.* 194:93.12

Porter LJ, Klimchuk JA. 1995. *Ap. J.* 454:499–511

Priest ER. 2000. *Astron. Soc. Pac. Conf. Ser.* 206:13–26

Priest ER, Foley CR, Heyvaerts J, Arber TD, Culhane JL, Acton L. 1998. *Nature* 393:545–47

Priest ER, Foley CR, Heyvaerts J, Arber TD, MacKay D, et al. 2000. *Ap. J.* 539:1002–22

Priest ER, Forbes T. 2000. *Magnetic Reconnection. MHD Theory and Applications*. Cambridge, UK: Cambridge Univ. Press

Qiu J, Wang H, Chae J, Goode PR. 1999. *Sol. Phys.* 190:153–65

Rabin D. 1991. *Ap. J.* 383:407–19

Ramaty R, Mandzhavidze N. 1999. *IAU Coll.* 195:123–32

Ramaty R, Mandzhavidze N. 2000. *High Energy Solar Physics—Anticipating HESSI. Astron. Soc. Pac. Conf. Ser.*, Vol. 206. San Francisco: Astron. Soc. Pac.

Raymond J, Kohl JL, Noci G, Antonucci E, Tondello G, et al. 1997. *Sol. Phys.* 175:645–65

Reale F, Peres G. 2000. *Ap. J.* 528:L45–48

Reale F, Peres G, Serio S, Betta RM, DeLuca EE, Golub L. 2000a. *Ap. J.* 535:423–37

Reale F, Peres G, Serio S, DeLuca EE, Golub L. 2000b. *Ap. J.* 535:412–22

Reames DV. 1999. *Space Sci. Rev.* 90(3/4):413–91

Roald CB, Sturrock PA, Wolfson R. 2000. *Ap. J.* 538:960–67

Roberts B. 2000. *Sol. Phys.* 193:139–52

Roberts B, Edwin PM, Benz AO. 1984. *Ap. J.* 279:857–65

Rosner R, Tucker WH, Vaiana GS. 1978. *Ap. J.* 220:643–65

Rust DM. 1999. *Magnetic Helicity in Space and Laboratory Plasmas. Geophys. Monogr.*, 111:221. Washington, DC: Am. Geophys. Union

Rust DM. 2000. In *Proc. IAU Coll.* 179: In press

Rust DM, Kumar A. 1996. *Ap. J.* 464:L199–202

Ryutova MP, Habbal S, Woo R, Tarbell T. 2001. *Sol. Phys.* In press

Ryutova MP, Tarbell TD. 2000. *Ap. J.* 541:L29–32

Sakai JK, DeJager C. 1996. *Space Sci. Rev.* 77:1–192

Sakai JK, Kawata T, Yoshida K, Furusawa K, Cramer NF. 2000. *Ap. J.* 537:1063–72

Schmelz JT, Holman GD, Brosius JW, Gonzalez RD. 1992. *Ap. J.* 399:733–42

Schmieder B, Delannée C, Yong DY, Vial JC, Madjarska M. 2000. *Astron. Astrophys.* 358:728–40

Schmieder B, Heinzel P, Kucera T, Vial JC. 1998. *Sol. Phys.* 181:309–26

Schrijver CJ. 2001. *Proc. 11th Workshop on Cool Stars, Stellar Systems and the Sun. Astron. Soc. Pac. Conf. Ser.*, ed. G Lopez, R Rebolo, MR Zapatero Osorio, San Francisco: Astron. Soc. Pac. 223:131–44

Schrijver CJ. 2001. *Sol. Phys.* 198:325–49

Schrijver CJ, Brown DS. 2000. *Ap. J.* 537:L69–72

Schrijver CJ, Title AM, Berger TE, Flectcher L, Hurlburt NE, et al. 1999. *Sol. Phys.* 187:261–302

Serio S, Peres G, Vaiana GS, Golub L, Rosner R. 1981. *Ap. J.* 243:288–300

Sheeley NR Jr, Howard RA, Koomen MJ, Michels DJ. 1983. *Ap. J.* 272:349–54

Sheeley NR Jr, Howard RA, Koomen MJ, Michels DJ. 1997. *Ap. J.* 484:472–78

Sheeley NR Jr, Walters JH, Wang YM, Howard RA. 1999. *J. Geophys. Res.* 104(A11):24739–68

Shibata K, Ishido Y, Acton LW, Stroug KT, Hirayama T, et al. 1992. *PASJ* 44:L173–80

Shibata K, Masuda S, Shimojo M, Hara H, Yokoyama T, et al. 1995. *Ap. J.* 451:L83–86

Shimizu T, Tsuneta S. 1997. *Ap. J.* 486:1045–57
Shimizu T, Tsuneta S, Acton LW, Lemen JR, Uchida Y. 1992. *PASJ* 44:L147–53
Shimojo M, Hashimoto S, Shibata K, Hirayama T, Hudson HS, Acton LW. 1996. *PASJ* 48:123–36
Singh J, Sakurai T, Ichimoto K, Hiei E. 1999. *Bull. Astron. Soc. India* 28:33
Spadaro D. 1999. *Proc. 9th Eur. Meet. Sol. Phys.*, ed. A Wilson, Noordwijk, Netherlands: Eur. Spa. Agy. 448:157–65
Sterling AC. 1999. *Astron. Astrophys.* 346:995–1002
Sterling AC, Hudson HS. 1997. *Ap. J.* 491:L55–58
Sterling AC, Pike CD, Mason HE, Watanabe T, Antiochos S. 1999. *Ap. J.* 524:1096–104
Strachan L, Panasyuk AV, Dobrzycka D, Kohl J, Noci G, et al. 2000. *J. Geophys. Res.* 105:2345S
Strong KT, Saba JLR, Haisch BM, Schmelz JT, eds. 1999. *The Many Faces of the Sun: A Summary of the Results from NASA's Solar Maximum Mission*. New York: Springer. 610 pp.
Sturrock PA. 1996. *Ap. J.* 461:L115–18
Sturrock PA. 1999. *Ap. J.* 521:451–59
Sturrock PA, Roald CB, Wolfson R. 1999. *Ap. J.* 524:L75–78
Sturrock PA, Wheatland MS, Acton LW. 1996. IAU Coll. 153:417
Su QR, Su M. 2000. *Sol. Phys.* 194:121–30
Tang YH, Mouradian Z, Schmieder B, Fang C, Sakurai T. 1999. *Sol. Phys.* 185:143–55
Tappin SJ, Simnett GM, Lyons MA. 1999. *Astron. Astrophys.* 350:302–9
Tarbell TD, Ryutova M, Covington J, Fludra A. 1999. *Ap. J.* 514:L47–51
Tarbell TD, Ryutova M, Shine R. 2000. *Sol. Phys.* 193:195–218
Thompson BJ, Gurman JB, Neupert WM, Newmark JS, Delaboudiniere JP, et al. 1999. *Ap. J.* 517:L151–54
Thompson BJ, Plunkett SP, Gurman JB, Newmark JS, St. Cyr OC, et al. 1998. *Geophys. Res. Lett.* 25(14):2461–64
Thompson BJ, Reynolds B, Aurass H, Gopalswamy N, Gurman JB, et al. 2000. *Sol. Phys.* 193:161–80
Tousey R. 1973. *Adv. Space Res.* 13:713
Tsiropoula G, Alissandrakis CE, Mein P. 2000. *Astron. Astrophys.* 355:375–80
Tsuneta S. 1996. *Ap. J.* 456:L63–65
Uchida Y, Fujisaki K, Morita S, Torii M, Hirose S, Cable S. 1999. *Publ. Astr. Soc. Jpn.* 51:53–61
VanBallegooijen AA, Cartledge NP, Priest ER. 1998. *Ap. J.* 501:866–81
VanBallegooijen AA, Deluca EE. 1999. *Am. Astron. Soc. Meet.* 194:78.06
VanBallegooijen AA, Priest ER, MacKay DH. 2000. *Ap. J.* 539:983–94
VanDriel-Gestzelyi L, Schmieder B, Aulanier G, Demoulin P, Morteas PCH, et al. 1998. *Astron. Soc. Pac. IAU Coll.* 167 150:366–69
Vassiliadis D, Anastasiadis A, Georgoulis M, Vlahos L. 1998. *Ap. J.* 509:L53–56
Vlahos L. 1994. *Space Sci. Rev.* 68:39–51
Vlahos L, Georgoulis M, Kluiving R, Paschos P. 1995. *Astron. Astrophys.* 299:897–911
Wang JX, Li W, Denker C, Lee C, Wang H, et al. 2000. *Ap. J.* 530:1071–84
Wang YM, Sheeley NR. 1999. *Ap. J.* 510: L157–60
Wang YM, Sheeley NR, Socker DG, Howard RA, Brueckner GE, et al. 1998b. *Ap. J.* 508:899–907
Wang YM, Sheeley NR, Walter JH, Brueckner GE, Howard RA, et al. 1998a. *Ap. J.* 498:L165–68
Warren HP. 1999. *Sol. Phys.* 190:363–77
Warren HP. 2000. *Ap. J.* 536:L105–8
Watanabe T, Kosugi T, Sterling AC, eds. 1998. *Observational Plasma Astrophysics: Five Years of Yohkoh and Beyond*. Dordrecht, Ger.: Kluwer
Webb DF, Howard RA. 1994. *J. Geophys. Res.* 99:4201–20
Webb DF, Kahler SW, McIntosh PS, Klimchuk JA. 1997. *Geophys. Res.* 192(A11):24161–74
Wheatland MS, Sturrock PA, Acton LW. 1997. *Ap. J.* 482:510–18

Wikstol O, Hansteen VH, Carlsson M, Judge PG. 2000. *Ap. J.* 531:1150–60

Wilhelm K, Marsch E, Dwivedi BN, Hassler DM, Lemaire P, et al. 1998. *Ap. J.* 500:1023–38

Wills-Davey MJ, Thompson BJ. 1999. *Sol. Phys.* 190:467–83

Winebarger AR, Emslie AG, Mariska JT, Warren HP. 1999. *Ap. J.* 526:471–77

Withbroe GL, Noyes RW. 1997. *Annu. Rev. Astron. Astrophys.* 15:363–87

Wolfson R, Roald CB, Sturrock PA, Lemen JR, Shirts P. 2000. *Ap. J.* 529:570–74

Wood BE, Karovska M, Chen J, Brueckner GE, Cook JW, Howard RA. 1999. *Ap. J.* 512:484–95

Young PR, Klimchuk JA, Mason HE. 1999. *Astron. Astrophys.* 350:286–301

Zhang J, White SM, Kundu MR. 1999. *Ap. J.* 527:977–91

Zirker JB, Engvold O, Martin SF. 1998. *Nature* 396:440–41

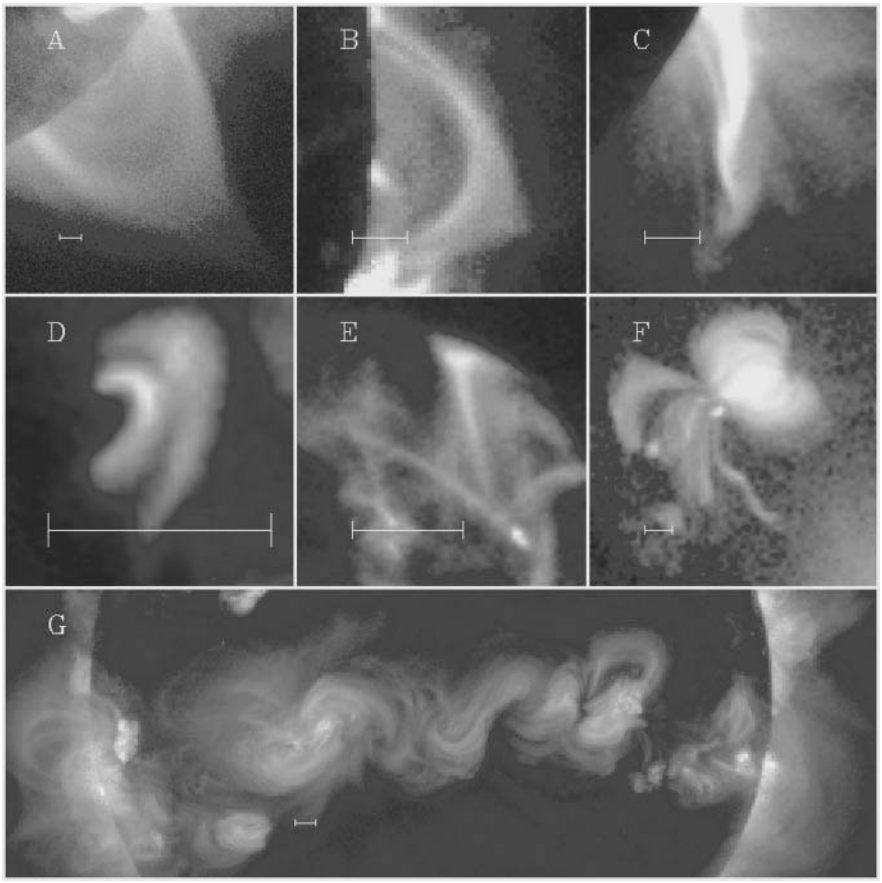

Figure 3 Examples of magnetic structures observed with Yohkoh: (*A*) helmet-shaped arch, (*B*) arcade of X-ray loops, (*C*) eruptive feature, (*D*) quadrupolar pair of flare loops, (*E*) cusped loops, (*F*) "bow-tie" structure, and (*G*) chain of S-shaped active region loops. (*Horizontal bars*) 1 arcmin (43,500 km). (Courtesy Acton et al. 1992)

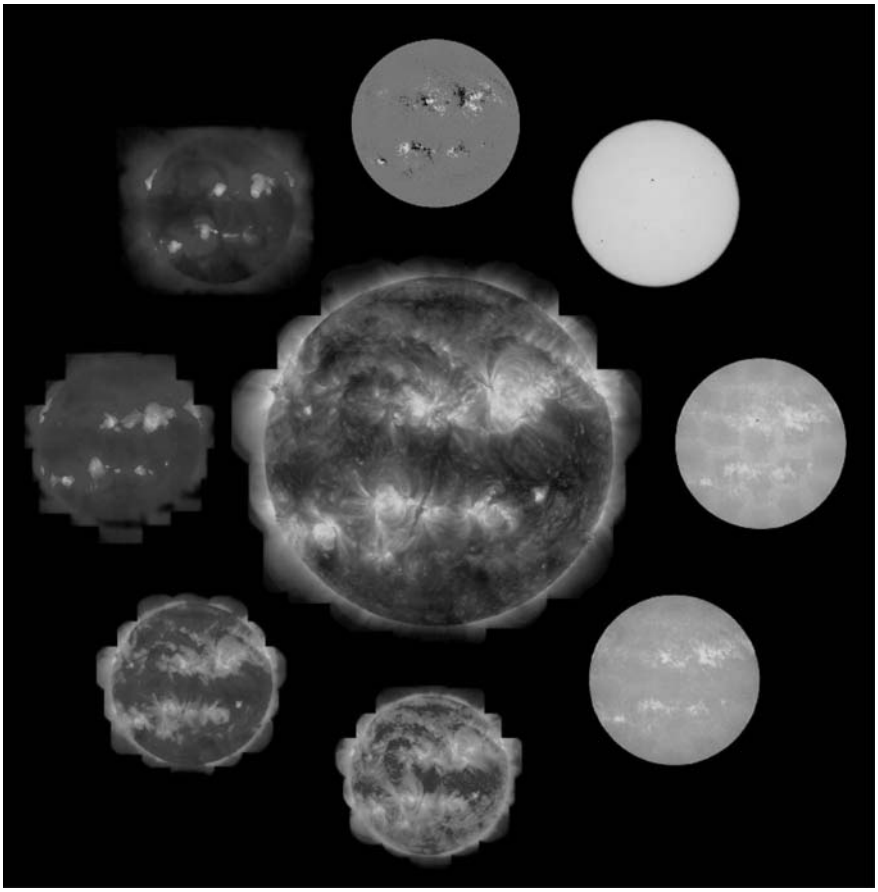

Figure 4 The multitemperature structure of the solar corona is visualized with images in different wavelengths. The central part is composed of a mosaic with three exposures at each of 23 pointings, observed by TRACE in 171 Å (1 MK), 195 Å (1.5 MK), and 284 Å (2 MK) on 29 June 1999, 02 UT. The peripheral solar images, starting at the *top* and in *clockwise direction* are MDI magnetogram, white-light, 1600 Å, Ly α, 171 Å, 195 Å, 284 Å, and a Yohkoh image (2–4 MK). (Courtesy Lockheed-Martin Solar and Astrophysics Laboratory)

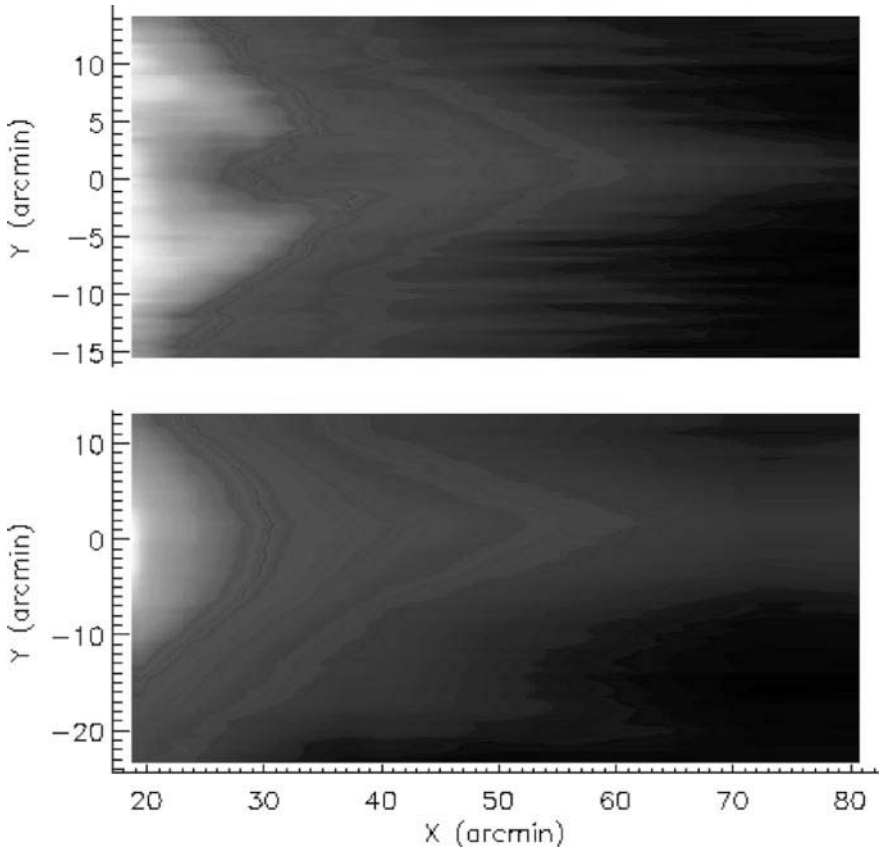

Figure 5 Ultraviolet coronagraph spectrometer observations of an equatorial streamer above the west limb on 12 Oct 1996. (*Lower panel*) The same streamer in the light from neutral hydrogen atoms (HI Lyman α) at 121.6 nm. (Courtesy JC Raymond)

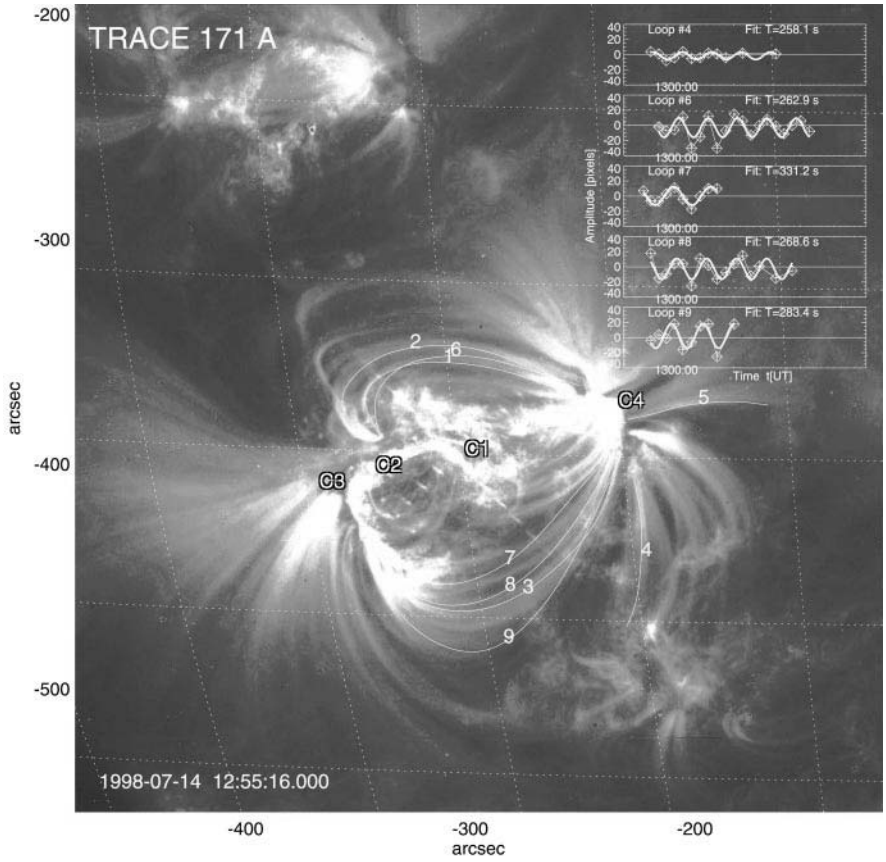

Figure 7 TRACE 171 Å observations of the 14 July 1998, 12:55 UT, flare. A set of coronal loops is marked, of which five were found to exhibit transverse oscillations (4, 6, 7, 8, 9), while the others displayed only a transverse displacement at the start of the flare. (*Insert*) The amplitude of the transverse oscillations, corresponding to distances of ≈ 4 Mm, whereas the loops have a mean length of ≈ 130 Mm. (Courtesy Aschwanden et al. 1999c)

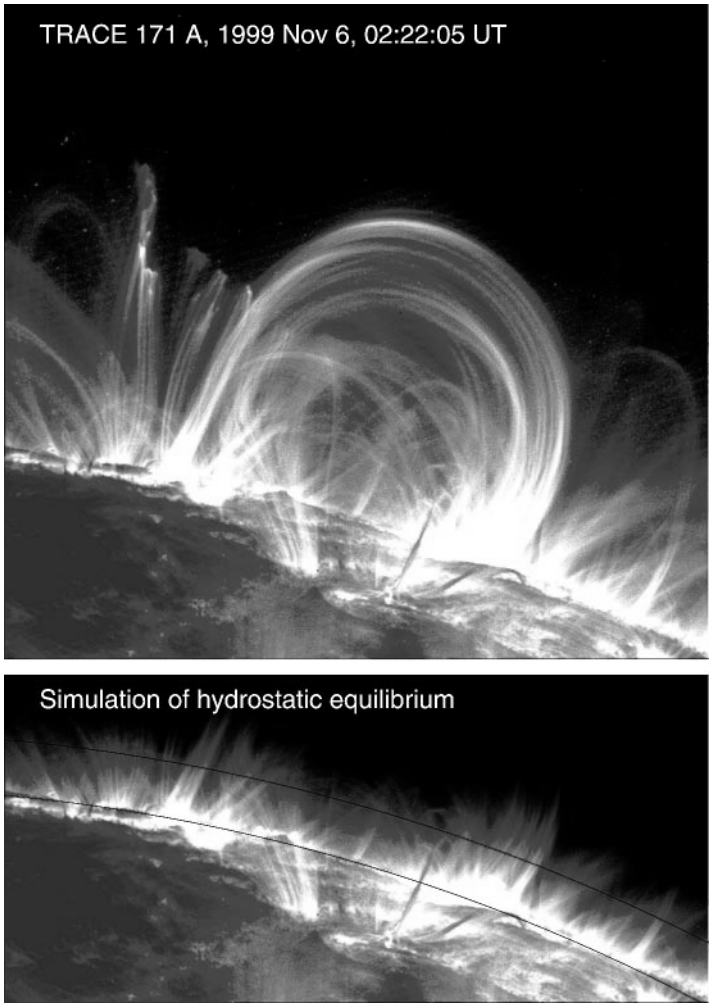

Figure 8 (*Top*) TRACE observations of active-region loops at the east limb (rotated by 90°) of NOAA AR 8759 on 6 November 1999, 02:22:05 UT, at a wavelength of 171 Å (1.0 MK). A GOES-class M3.0 flare occurred 8 h earlier in this active region, on 5 November, 18:04 UT. Note that most of the loops are filled with detectable plasma up to the loop tops, which is not expected if these loops were in hydrostatic equilibrium. Energy balance requires nonuniform heating confined to low altitudes of $h \lesssim 16$ Mm, although the loops have apex heights of $\lesssim 150$ Mm. (*Bottom*) Simulation of the same active region in hydrostatic equilibrium, according to a density scale height of $\lambda_{\rm T} = 47$ Mm for the $T = 1.0$ MK plasma. The corresponding flux scale height is $\lambda_{\rm F} = \lambda_{\rm T}/2 = 23$ Mm (*black curve*), because the flux F is proportional to the emission measure (EM) or squared density n_e^2, ($F \propto EM \propto n_e(h)^2$). (Adapted from Aschwanden et al 2001)

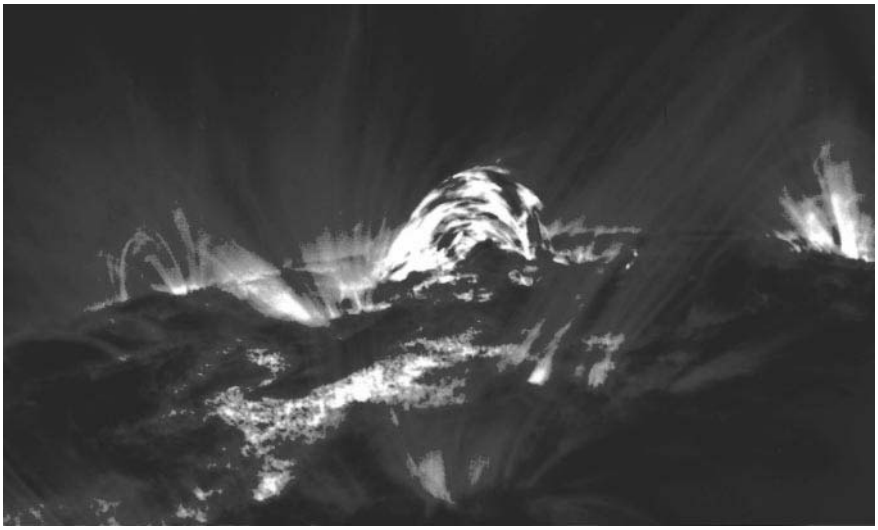

Figure 10 This TRACE image of active region 9169 shows a filament activation that occurred around 23:53 UT (probably associated with a C2.9 flare) on 29 September 2000. The small filament (compare the image of the quiescent filament just before the activation) rose up and showed a tangled web of bright and dark strands, in which material moves in either direction. Things gradually quieted down, and after a few hours all was as quiet as before. (Courtesy TRACE/LMSAL team)

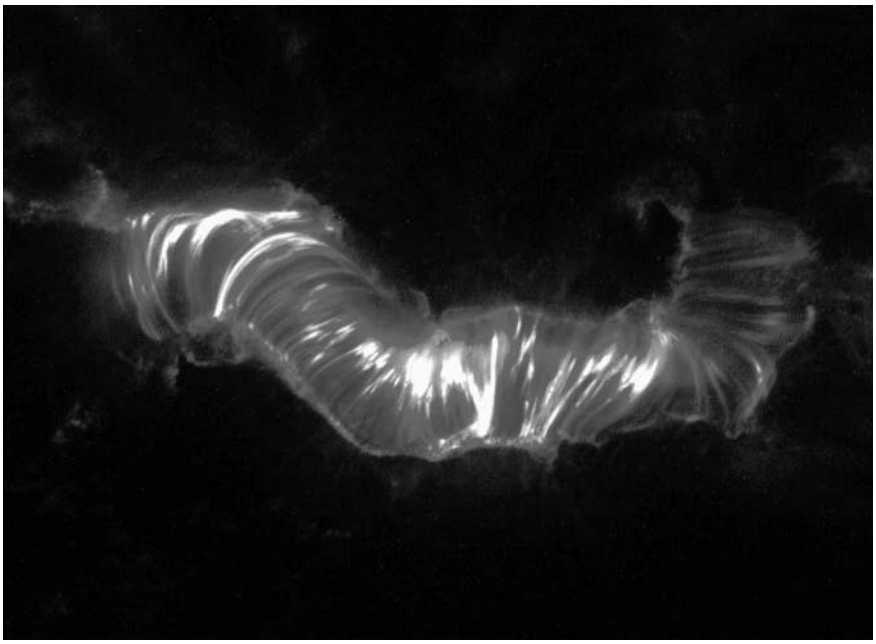

Figure 11 A major solar flare produces an arcade resembling a slinky. The X5.7 flare occurred at 10:03 UT on 14 July 2000, in active region 9077, observed by TRACE in its 195 Å pass band. A filament in the center of the region destabilized and was seen to lift off. Following this mass ejection, an arcade of magnetic field lit up and cooled down from many millions of degrees. (See the 6.8 MB Quicktime [Photo(JPEG)-compressed] movie to see the evolution of the magnetic arcade.) Note that the exposures have been rescaled to the same peak intensity to show the evolution of the central bright region. This causes the surroundings of the flare site to apparently dim markedly as the flare reaches peak brightness. The field of view is 230,000 by 170,000 km. (Courtesy TRACE/LMSAL team)

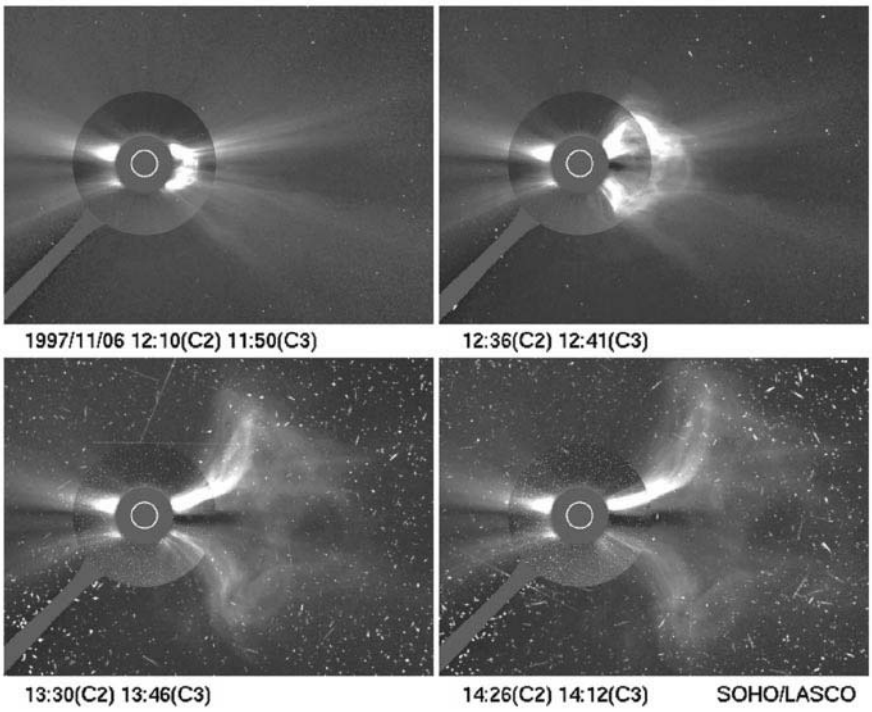

Figure 12 SoHO/LASCO images of a coronal mass ejection on 6 November 1997, 12:10–14:26 UT, followed by a particle shower that hit the SoHO spacecraft after 13:30 UT. (See related LASCO movie)

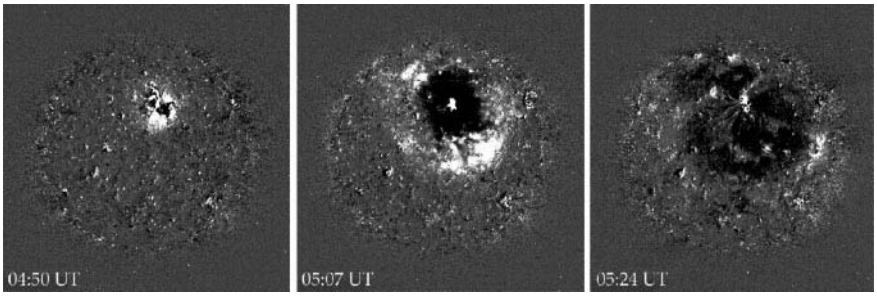

Figure 13 Extreme ultraviolet imaging telescope (EIT) observations of EIT waves, the coronal analog to Moreton waves, expanding from a coronal mass ejection initiation on 12 May 1997. The images represent time differences taken in Fe XII, 195 Å (1.5 MK). Note the global spreading within half an hour. (Courtesy Barbara Thompson and EIT team)